Atmos. Chem. Phys., 22, 11323–11346, 2022
https://doi.org/10.5194/acp-22-11323-2022

Atmospheric Chemistry and Physics
Open Access
EGU

Identification of highly oxygenated organic molecules and their role in aerosol formation in the reaction of limonene with nitrate radical

Yindong Guo[1], Hongru Shen[1], Iida Pullinen[2,a], Hao Luo[1,3], Sungah Kang[2], Luc Vereecken[2], Hendrik Fuchs[2], Mattias Hallquist[4], Ismail-Hakki Acir[2,b], Ralf Tillmann[2], Franz Rohrer[2], Jürgen Wildt[2], Astrid Kiendler-Scharr[2], Andreas Wahner[2], Defeng Zhao[1,5,6], and Thomas F. Mentel[2]

[1]Department of Atmospheric and Oceanic Sciences & Institute of Atmospheric Sciences, Fudan University, Shanghai 200438, China
[2]Institute of Energy and Climate Research, IEK-8: Troposphere, Forschungszentrum Jülich GmbH, 52425 Jülich, Germany
[3]IRDR ICoE on Risk Interconnectivity and Governance on Weather/Climate Extremes Impact and Public Health, Fudan University, Shanghai 200438, China
[4]Department of Chemistry and Molecular biology, University of Gothenburg, Göteborg 41258, Sweden
[5]Shanghai Frontiers Science Center of Atmosphere–Ocean Interaction, Fudan University, Shanghai 200438, China
[6]Institute of Eco-Chongming (IEC), 20 Cuiniao Rd., Chongming, Shanghai 202162, China
[a]now at: Department of Applied Physics, University of Eastern Finland, Kuopio 70210, Finland
[b]now at: Institute of Nutrition and Food Sciences, University of Bonn, 53115 Bonn, Germany

Correspondence: Defeng Zhao (dfzhao@fudan.edu.cn) and Thomas F. Mentel (t.mentel@fz-juelich.de)

Received: 29 January 2022 – Discussion started: 4 February 2022
Revised: 22 July 2022 – Accepted: 9 August 2022 – Published: 2 September 2022

Abstract. Nighttime NO_3-initiated oxidation of biogenic volatile organic compounds (BVOCs) such as monoterpenes is important for the atmospheric formation and growth of secondary organic aerosol (SOA), which has significant impact on climate, air quality, and human health. In such SOA formation and growth, highly oxygenated organic molecules (HOM) may be crucial, but their formation pathways and role in aerosol formation have yet to be clarified. Among monoterpenes, limonene is of particular interest for its high emission globally and high SOA yield. In this work, HOM formation in the reaction of limonene with nitrate radical (NO_3) was investigated in the SAPHIR chamber (Simulation of Atmospheric PHotochemistry In a large Reaction chamber). About 280 HOM products were identified, grouped into 19 monomer families, 11 dimer families, and 3 trimer families. Both closed-shell products and open-shell peroxy radicals ($RO_2^{\bullet}$) were observed, and many of them have not been reported previously. Monomers and dimers accounted for 47 % and 47 % of HOM concentrations, respectively, with trimers making up the remaining 6 %. In the most abundant monomer families, $C_{10}H_{15-17}NO_{6-14}$, carbonyl products outnumbered hydroxyl products, indicating the importance of $RO_2^{\bullet}$ termination by unimolecular dissociation. Both $RO_2^{\bullet}$ autoxidation and alkoxy–peroxy pathways were found to be important processes leading to HOM. Time-dependent concentration profiles of monomer products containing nitrogen showed mainly second-generation formation patterns. Dimers were likely formed via the accretion reaction of two monomer $RO_2^{\bullet}$, and HOM-trimers via the accretion reaction between monomer $RO_2^{\bullet}$ and dimer $RO_2^{\bullet}$. Trimers are suggested to play an important role in new particle formation (NPF) observed in our experiment. A HOM yield of $1.5\,\%^{+1.7\,\%}_{-0.7\,\%}$ was estimated considering only first-generation products. SOA mass growth could be reasonably explained by HOM condensation on particles assuming irreversible uptake of ultra-low volatility organic compounds (ULVOCs), extremely low volatility organic compounds (ELVOCs), and low volatility organic compounds (LVOCs). This

work provides evidence for the important role of HOM formed via the limonene $+NO_3$ reaction in NPF and growth of SOA particles.

1 Introduction

The nitrate radical (NO_3) is an important nighttime oxidant in tropospheric chemistry, and can reach mixing ratios of several hundred pptv during nighttime (Seinfeld and Pandis, 2006). It can react with volatile organic compounds (VOCs) and is especially reactive to alkenes, where the nitrate radical can undergo an addition reaction to the C=C double bond (Finlayson-Pitts and Pitts, 1997; Seinfeld and Pandis, 2006). Biogenic monoterpenes ($C_{10}H_{16}$) are a large contribution to the alkenes in the atmosphere (Klinger et al., 2002; Guenther et al., 2012), and their major nighttime loss pathway is reaction with NO_3 (Beaver et al., 2012; Rollins et al., 2012; Ayres et al., 2015; Fry et al., 2013). The chemistry of monoterpenes with NO_3 has implications on the cycle of reactive nitrogen and thus on ozone formation (Brown and Stutz, 2012). Furthermore, since the NO_3 radical is formed through the reaction of NO_2 with O_3, it is considered to be of anthropogenic origin, and reactions of NO_3 with biogenic VOC (BVOC) thus represent an important interaction between biogenic emissions and anthropogenic emissions.

The reaction of NO_3 with monoterpenes can form secondary organic aerosols (SOAs), which can have a large impact on global climate, air quality, and human health (Hallquist et al., 2009; Shrivastava et al., 2017). Laboratory studies showed that monoterpenes have high SOA yields in the reaction with NO_3 due to the low volatility of oxidation products (Ng et al., 2008; Rollins et al., 2009; Fry et al., 2013, 2014; Ayres et al., 2015; Jokinen et al., 2015; Zhou et al., 2015; Boyd et al., 2015; Nah et al., 2016; Boyd et al., 2017; Slade et al., 2017; Claflin and Ziemann, 2018; Bates et al., 2022; Dam et al., 2022). Field studies also showed that nighttime NO_3-initiated oxidation of monoterpenes contributes significantly to SOA in forested regions influenced by anthropogenic emissions (Pye et al., 2010; Rollins et al., 2012; Fry et al., 2013; Ayres et al., 2015; Zhou et al., 2015; Xu et al., 2015; Lee et al., 2016; Zhang et al., 2018; Chen et al., 2020) and potentially in urban areas due to the extensive usage of so-called volatile chemical products (VCPs) (Nazaroff and Weschler, 2004; McDonald et al., 2018). For example, the Southern Oxidant and Aerosol Study (SOAS) showed that the BVOC+NO_3 reactions were a substantial source of SOA (Ayres et al., 2015; Xu et al., 2015; Lee et al., 2016; Massoli et al., 2018). Therefore, accurate predictions and evaluations of SOA concentration and thus its climate and environmental effects require a comprehensive understanding of the reactions of monoterpenes with NO_3.

Recently, a class of organic compounds named highly oxygenated molecules (HOM) have been shown to be critical substances in the SOA formation from BVOC oxidation, particularly monoterpenes, featuring high O/C ratio and low to extremely low volatility (Ehn et al., 2014; Tröstl et al., 2016; Kirkby et al., 2016; Bianchi et al., 2019). HOM here refers to compounds formed in the gas phase via autoxidation which contain at least six oxygen atoms (Bianchi et al., 2019). Most HOM are classified as ULVOC/ELVOC or LVOC (Bianchi et al., 2019) according to the classification of atmospheric organics based on their volatility (saturation concentration, C^*) by Donahue et al. (2012) (extremely low volatility organic compounds, ELVOCs; low volatility organic compounds, LVOCs; semi-volatile organic compounds, SVOCs; intermediate volatility organic compounds, IVOCs; volatile organic compounds, VOCs), and a recent update by Schervish and Donahue (2020) (ultra-low volatility organic compounds, ULVOCs). Thus, HOM can be a substantial contribution to growth of SOA particles through gas–particle partitioning.

A better description of the HOM formation chemistry in the oxidation of monoterpenes by NO_3 will improve our understanding of the role of HOM in SOA formation, and the relationship between oxidation products, SOA formation, and reaction systems. Field observation campaigns and laboratory experiments have proven the important contribution of HOM in monoterpene $+NO_3$ SOA (Lee et al., 2016; Faxon et al., 2018). In the SOAS campaign, HOM-ON (organic nitrates) were identified in both gas and particle phase using a NO_3^--chemical ionization time-of-flight mass spectrometer (CI-APi-TOF) and a high-resolution time-of-flight chemical ionization mass spectrometer (HR-ToF-CIMS) coupled to a Filter Inlet for Gases and AEROsols (FIGAERO). Species with the sum formula $C_{10}H_{15,17,19}NO_{4-11}$ were observed, which are formed through the oxidation of monoterpenes by NO_3 (Lee et al., 2016; Massoli et al., 2018). In a campaign in a boreal forest in Hyytiälä, measurement using a NO_3^--CI-APi-TOF and positive matrix factor (PMF) analysis showed a nighttime factor of HOM-ON formed via NO_3 oxidation of monoterpenes (Yan et al., 2016). Besides the observations at forested regions, monoterpene-derived HOM via NO_3 oxidation also contribute to organic aerosols in urban regions. For example, Liu et al. (2021) and Nie et al. (2022) have found that HOM derived from monoterpene nighttime chemistry are important in megacities in China, especially during summertime. A number of laboratory studies have reported HOM formation by the oxidation of monoterpenes with NO_3. Boyd et al. (2015) observed $C_{10}H_{17}NO_{4/5}$ and $C_{10}H_{15}NO_{5/6}$ in the gas phase in β-pinene $+NO_3$ experiments using a quadrupole chemical ionization mass spectrometer with I^- as the reagent

ion (I^--CIMS). They proposed possible formation schemes of these ONs. Nah et al. (2016) further detected 5 and 41 HOM-ON in the NO_3 oxidation of α-pinene and β-pinene, respectively, such as $C_{10}H_{15/17/19}NO_{4-9}$ in the gas- and particle-phase using I^--FIGAERO HR-ToF-CIMS. Claflin and Ziemann (2018) provided formation mechanisms for HOM-ON via gas-phase and particle-phase reactions in the β-pinene $+NO_3$ reaction system, where particle-phase products were analyzed using reversed-phase high-performance liquid chromatography equipped with a UV–vis photodiode array detector (HPLC-UV), electron-ionization thermal desorption particle beam mass spectrometer (EI-TDPBMS), chemical ionization Finnigan PolarisQ ion trap mass spectrometer (CI-ITMS), and electrospray-ionization mass spectrometer (ESI-MS). Recently, Shen et al. (2021) found a large number of HOM (> 150 species) in the β-pinene $+NO_3$ reaction using NO_3^--CI-APi-TOF. HOM formed in the reaction of four monoterpenes (α-pinene, β-pinene, Δ-3-carene, and α-thujene) with NO_3 were also detected using NO_3^--CI-APi-TOF by Dam et al. (2022). Bell et al. (2021) found that dimer dinitrates ($C_{20}H_{32}N_2O_{8-13}$) contribute a large portion to SOA from α-pinene $+NO_3$, and also detected monomer ON such as $C_{10}H_{15}NO_{5-10}$ and $C_{10}H_{14,16}N_2O_{7-11}$) using FIGAERO-CIMS and an extractive electrospray ionization time-of-flight mass spectrometer (EESI-ToF-MS). However, the detailed speciation depends on analytical method to some extent. Moreover, the HOM composition in the particle-phase was found to depend on aging time and reaction conditions such as dark versus light (Bell et al., 2021; C. Wu et al., 2021).

Among the monoterpenes, understanding the reaction system of limonene with NO_3 is of specific importance. The emission of limonene makes the fourth largest contribution with an estimated global emission of 11.4 Tg annually, preceded only by α-pinene, trans-β-ocimene, and β-pinene (Guenther et al., 2012). Besides its biogenic origin, limonene is also a common additive in cleaning products (Nazaroff and Weschler, 2004) and can even be used as a tracer for fragrances in some places (Gkatzelis et al., 2021). Several studies have shown adverse health effects due to indoor pollution caused by the ozonolysis of limonene (Clausen et al., 2001; Fan et al., 2003; Carslaw et al., 2012; Pagonis et al., 2019). Moreover, limonene stands out with its high reactivity towards the NO_3 radical (with a lifetime of 3 min at 298 K at 20 pptv NO_3) (Ziemann and Atkinson, 2012), and NO_3 oxidation of limonene has high SOA yield (SOA mass yield 15 % to 231 %) (Hallquist et al., 1999; Spittler et al., 2006; Fry et al., 2011, 2014; Boyd et al., 2017; Berkemeier et al., 2020; Mutzel et al., 2021). A number of earlier studies have provided valuable insights into the reaction of limonene with NO_3 regarding its main products and their formation pathways, the SOA yield, and the SOA physicochemical properties. For example, Hallquist et al. (1999) measured the SOA mass yield and revealed the dominance of organic nitrates (ONs) and carbonyl compounds in the products. Fry et al. (2011) determined the organic nitrate yield and proposed a reaction scheme leading to the formation of ON and carbonyls, and Fry et al. (2014) compared the SOA and ON yields from the NO_3 oxidation of α-pinene, β-pinene, and limonene, and demonstrated why limonene $+NO_3$ leads to more SOA and ON than α-pinene from a structural perspective. Boyd et al. (2017) found a higher N : C ratio for limonene $+NO_3$ SOA than for β-pinene $+NO_3$ SOA. Finally, Peng et al. (2018) studied the optical properties of the limonene $+NO_3$ SOA.

Regarding the HOM formation in the reaction of limonene with NO_3, Faxon et al. (2018) reported a series of HOM in the particle phase, including C_{7-10} monomers with 3–11 oxygen atoms and C_{11-20} dimers with 5–19 oxygen atoms using I^--FIGAERO HR-ToF-CIMS. However, identification of gas-phase HOM products in the limonene $+NO_3$ reaction is still lacking and their formation mechanisms remain unclear. Theoretical investigations have revealed that NO_3 addition on the endocyclic C=C double bond is more favorable than the exocyclic one due to a lower energy barrier (Jiang et al., 2009), and this endocyclic double bond of limonene thus tends to be attacked by NO_3 and leads to products including hydroxy-substituted ON or diketone products. The remaining exocyclic double bond can also be attacked by NO_3 in secondary chemistry, leading to more functionalized products (Fry et al., 2011).

The formation of HOM via autoxidation involves a sequence of multiple intramolecular H-shift and O_2 addition reactions, and results in highly oxygenated peroxy radicals (HOM-$RO_2^\bullet$) (Ehn et al., 2014). These HOM-$RO_2^\bullet$ can react similarly to traditional $RO_2^\bullet$ (Bianchi et al., 2019). The bimolecular reactions of HOM-$RO_2^\bullet$ with $RO_2^\bullet$, $HO_2^\bullet$, and NO lead to highly oxidized closed shell products including carbonyls, hydroperoxides, alcohols, or organic nitrates as termination groups (Reactions R1 to R3), or form accretion products (Reaction R4) (Ehn et al., 2014; Mentel et al., 2015). Unimolecular termination reactions of HOM-$RO_2^\bullet$ lead to carbonyls or epoxides (reactions R5 to R6) (Crounse et al., 2013). On the other hand, reactions of HOM-$RO_2^\bullet$ with NO, $RO_2^\bullet$, NO_3 at nighttime can lead to alkoxy radicals as chain propagating steps (reactions R7 to R9):

$$RO_2^\bullet + RO_2^\bullet \rightarrow R_HC{=}O + ROH + O_2 \quad \text{(R1)}$$

$$RO_2^\bullet + HO_2^\bullet \rightarrow ROOH + O_2 \quad \text{(R2)}$$

$$RO_2^\bullet + NO \rightarrow RONO_2 \quad \text{(R3)}$$

$$RO_2^\bullet + RO_2^\bullet \rightarrow ROOR + O_2 \quad \text{(R4)}$$

$$RO_2^\bullet \rightarrow R{=}O + OH \quad \text{(R5)}$$

$$RO_2^\bullet \rightarrow \text{epoxide} + OH \quad \text{(R6)}$$

$$RO_2^\bullet + NO \rightarrow RO^\bullet + NO_2 \quad \text{(R7)}$$

$$RO_2^\bullet + RO_2^\bullet \rightarrow RO^\bullet + RO^\bullet \quad \text{(R8)}$$

$$RO_2^\bullet + NO_3 \rightarrow RO^\bullet + NO_2 + O_2. \quad \text{(R9)}$$

If the reactive HOM-$RO^\bullet$ products undergo an H-migration reaction, they will again form HOM-RO_2 radicals ("alkoxy–

peroxy" pathway) (Mentel et al., 2015), continuing the autoxidation chain. Finally, the HOM-$RO^{\bullet}$ may also fragment leading to small RO_2 radicals, isomerize leading to carbonyls (Bianchi et al., 2019), or react with O_2 to form carbonyls (Ziemann and Atkinson, 2012).

In this study, HOM formation in the NO_3 oxidation of limonene was investigated. We report the identification of gas-phase HOM products, including monomers, dimers, and trimers. The formation pathways of dominant products in each category are proposed based on their time profiles in response to multiple additions of limonene in the experiment and on the information in literature. Based on this analysis, we estimated HOM yields, and discuss the role of HOM in nucleation and growth of SOA particles.

2 Experiment and methods

2.1 Experiment setup

The limonene $+NO_3$ experiment was performed in the atmospheric simulation chamber SAPHIR (Simulation of Atmospheric PHotochemistry In a large Reaction chamber) at the Forschungszentrum Jülich, Germany. SAPHIR is a 270 m^3 double-wall cylindrical Teflon chamber with a surface-to-volume ratio of $\sim 1\,m^2\,m^{-3}$. Details of SAPHIR have been described before (Rohrer et al., 2005; Zhao et al., 2015a, b; Zhao et al., 2018) and are only summarized here. Detailed experimental procedures can be found in Fig. 1a. Before each experiment, SAPHIR was flushed for about 4 h at a flow rate of $370\,m^3\,h^{-1}$ with high-purity synthetic air (purity > 99.9999 % O_2 and N_2) in order to clean the chamber. To simulate nighttime conditions for the NO_3 chemistry, the chamber roof remained closed throughout the experiment. The experiment was performed under dry conditions (RH < 2 %) at a temperature of 302 ± 3 K. No seed aerosols were used in the experiments. A fan was used for active mixing in the chamber, leading to a typical mixing time of ~ 1 min (Fuchs et al., 2013).

NO_3 radicals were generated via the reaction of ozone with nitrogen dioxide:

$$NO_2 + O_3 \rightarrow NO_3 + O_2, \quad \text{(R10)}$$

$$NO_2 + NO_3 \leftrightarrow N_2O_5. \quad \text{(R11)}$$

Therefore, O_3 and NO_2 were first added to the chamber to form N_2O_5 and NO_3 with mixing ratios of ~ 2 and ~ 0.15 ppbv, respectively. About 20 min later, 5 ppbv of limonene was added to start the organic chemistry. Five more additions of limonene followed, with added concentrations of about 3, 3, 2, 2, and finally 8 ppbv, which divided the experiment into six periods (P1 to P6) (Fig. 1a). For period P3 and P5, NO_2 and O_3 were also added to compensate for the loss of NO_3 and N_2O_5 (Fig. 1a). The concentrations of NO_2 and O_3 were maintained around 20 to 70 ppbv throughout the experiment, ensuring the major loss of limonene was by reaction with NO_3 rather than with O_3 (Figs. S1). In the first 10 min of reaction (named period P1a hereafter, Fig. 1a), NO_3 accounted for 86 % of the chemical loss of limonene.

2.2 Instrumentation

Gas-phase HOM were detected by a chemical ionization time-of-flight mass spectrometer (CI-APi-TOF, Aerodyne Research Inc., USA) with a resolution $(m/z)/(\Delta m/z)$ of ~ 3800 using $^{15}NO_3^-$ as the reagent ion, which is capable of detecting organic molecules with high oxygen content (Eisele and Tanner, 1993; Jokinen et al., 2012). The mass spectra were analyzed using the software Tofware (Tofwerk/Aerodyne) in Igor Pro (WaveMetrics, Inc.). Peak identification was conducted by a high-resolution analysis (examples shown in Fig. S2). We observed several peaks which were obviously products from the isoprene $+NO_3$ reaction, such as $C_5H_{10}N_2O_8^{\bullet} \cdot {}^{15}NO_3^-$ at m/z 289. Such peaks were present before the limonene oxidation reaction started, suggesting that these compounds preexisted in the chamber. These isoprene oxidation products were likely formed in an isoprene $+NO_3$ experiment performed 2 d before (Zhao et al., 2021) and released slowly from chamber walls due to their semi-volatile character. Their total concentration is less than 1 ppt. All the isoprene-HOM observed ($C_5H_9NO_{7,10}$, $C_5H_8N_2O_{8-10}$, $C_5H_{10}N_2O_8$, $C_5H_9N_3O_{9,10}$) are saturated and do not contain C=C double bond. The isoprene-HOM will not influence the reaction of limonene with NO_3 in this study. Therefore, they are not discussed as products from the limonene oxidation in our experiment. (However, we cannot exclude that they were partly generated from fragmentation in the limonene $+NO_3$ reaction.)

A set of instruments were used to measure other gas-phase species, including VOC, NO_x, O_3, NO_3, and N_2O_5 (Shen et al., 2021). Concentrations of NO_3 and N_2O_5 were measured in situ using a home-built diode laser-based, cavity ring-down spectrometer similar to the instrument described in the work by Wagner et al. (2011). The concentrations of limonene were measured using a proton transfer reaction time-of-flight mass spectrometer (PTR-TOF-MS, Ionicon Analytik, Austria). The SOA number concentration, surface concentration, and size distribution were detected by a scanning mobility particle sizer (SMPS, TSI DMA3081/TSI CPC3786) and a condensation particle counter (CPC, TSI3785). Temperature and relative humidity were continuously monitored throughout the experiment.

2.3 Determination of HOM concentration and "primary" HOM yield

HOM concentrations were obtained from the normalized signals to the total signals of the mass spectra (nc, normalized counts) by applying a calibration coefficient (C) of 2.5×10^{10} molecule cm^{-3} nc^{-1}. C was determined using H_2SO_4 as the charging efficiency of HOM and H_2SO_4 are consid-

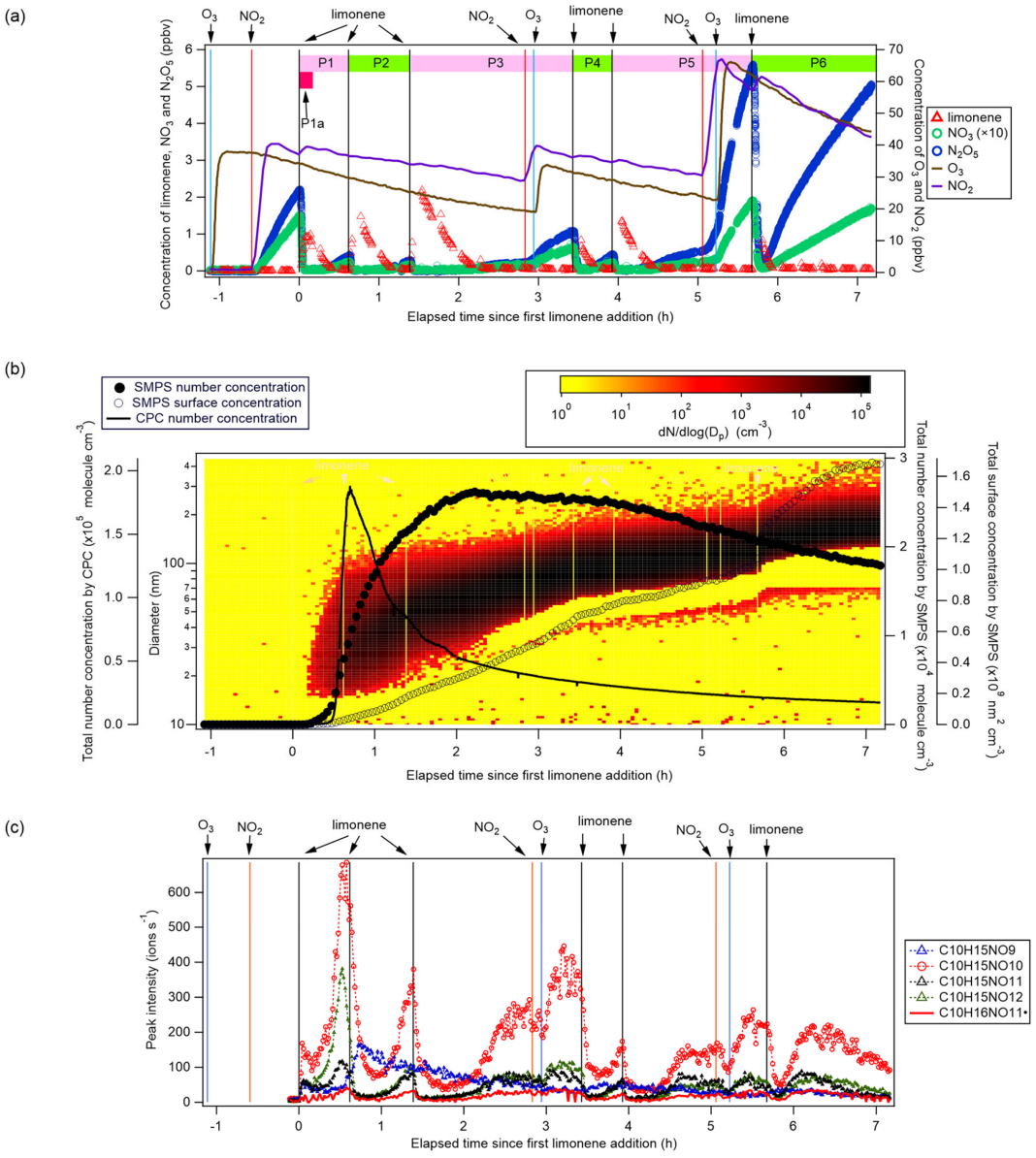

Figure 1. **(a)** Time series of the concentrations of limonene, NO_3, and N_2O_5 (left panel, the concentrations of NO_3 are magnified by a factor of 10 for clarity), and O_3 and NO_2 (right panel). The time periods P1 to P6 and P1a are also marked. **(b)** Total particle concentration and its size distribution during the whole period of experiment detected by SMPS and CPC. The solid and hollow black circles refer to total number concentration and total surface concentration detected by SMPS, respectively. Colors represent particle number concentration distribution based on $\log(D_p)$. The solid black line refers to total number concentration detected by CPC. **(c)** Time series of peak intensity of typical products of the $C_{10}H_{15}NO_x$ family and $C_{10}H_{16}NO^{\bullet}_{11}$ as a representative of the $C_{10}H_{16}NO^{\bullet}_{x}$ family. Vertical lines indicate the time of O_3 and NO_2 additions, and six limonene injections.

ered to be equal (Ehn et al., 2014; Pullinen et al., 2020; Shen et al., 2021). The details of determination of the calibration coefficient are shown in Sect. S1 in the Supplement. A mass-independent transmission efficiency was used according to our previous study, which causes an additional uncertainty of 14 % (Pullinen et al., 2020). In this previous study, the transmission efficiency curve of nitrate CI-APi-TOF was determined and found to monotonously decrease with increasing mass of ions but only slightly depend on the mass range (14 % change). As we used the same setting as our previous study, we have included the slight dependence of transmission on m/z in the uncertainties. The concentrations of HOM were corrected for chamber wall losses, which were determined for a number of HOM similar to our previous study (Zhao et al., 2018), with details described in the Supplement. When the chamber is actively mixed, the wall loss was deter-

mined to be $(2.2 \pm 0.2) \times 10^{-3}\ s^{-1}$. As the HOM yield was determined during the first 3 min of the experiment, we considered the wall loss rate to be constant ($2.2 \times 10^{-3}\ s^{-1}$) during this period. Sensitivity analysis showed that the HOM yield in this study is not very sensitive to the wall loss rate and is changing by only +0.88 % and −0.44 % if the wall loss rate is varied by +100 % or −50 %.

The HOM yield was calculated as

$$Y = \frac{[HOM]}{[VOC]_r} = \frac{I\,(HOM) \cdot C}{[N_2O_5]_r}, \quad (1)$$

where $[HOM]$ is the concentration of HOM, $I\,(HOM)$ is the total signal intensity of HOM, C is the calibration factor, and $[VOC]_r$ and $[N_2O_5]_r$ stand for the concentrations of limonene and N_2O_5 reacted, respectively. We used the reacted concentration of N_2O_5 rather than the measured reacted limonene concentration as a large fraction of limonene was already reacting away during the VOC injection before it was homogeneously mixed in the chamber. During this part of the experiment, the high limonene concentration resulted in a rapid loss of NO_3, such that every NO_3 formed from the decomposition of N_2O_5 reacted with limonene:

$$N_2O_5 \rightarrow NO_2 + NO_3 \quad (R12)$$

$$\text{limonene} + NO_3 \rightarrow \text{Products}. \quad (R13)$$

The initial NO_3 concentration before the limonene injection was small compared to the time-integrated loss of N_2O_5, and other NO_3 loss processes were negligible right after the limonene injection, so that the observed decrease in the N_2O_5 concentration equals indeed the consumption of limonene. The wall loss rate constant of N_2O_5 in the SAPHIR chamber is $7.2 \times 10^{-5}\ s^{-1}$ (Fry et al., 2009). As the HOM yield determination is based on the first 3 min, the wall loss of N_2O_5 can be ignored compared to the loss via the reaction of NO_3 with limonene.

The uncertainty of the HOM yield was estimated to be −55 %/ + 117 % based on the combined uncertainties of the HOM-ON peak intensities (∼ 10 %), the limonene concentration (∼ 15 %), the transmission efficiency (−0 %/ + 14 %), and the calibration factor (−52 %/ + 101 %) using error propagation (Zhao et al., 2021). The first 3 min after the injection of limonene were used to calculate the HOM yield, when most of the first-generation oxidation products were produced and negligible particles were formed. The HOM yield thus reflects the "primary" HOM yield.

2.4 Determination of HOM condensation on SOA

The SOA mass from the condensation of HOM was calculated to evaluate the role of HOM for the SOA mass growth. Detailed estimation methods are described in the Supplement, including the determination of particle wall loss and dilution loss rate (Sect. S2). In brief, the growth rate of SOA through HOM vapor condensation is based on the collision rate of vapor molecules with aerosols in the kinetic regime. The Fuchs–Sutugin approach is applied to describe the correction for transition from the kinetic to the diffusion regime (Fuchs and Sutugin, 1971; Ehn et al., 2014). Based on the volatility of HOM, we considered two scenarios for HOM condensation. In scenario 1, all HOM were assumed to irreversibly condense on the surface of particles leading to particle mass growth. In scenario 2, only the irreversible uptake of LVOC and ULVOC/ELVOC compounds were considered to contribute to the growth of SOA particles in order to examine the role of LVOC and ELVOC while IVOC and SVOC were not included, although they may also contribute to SOA. The calculation of saturation concentration C^* (in $\mu g\,m^{-3}$) of each HOM was done based on their molecular compositions using two different parameterizations considering the uncertainties in estimating volatility (R. Wu et al., 2021):

1. an updated version of the parameterization of Donahue et al. (2011) by Mohr et al. (2019) (scenario 2a):

$$\log_{10}(C) = (25 - n_C) \times 0.475 - (n_O - 3n_N) \times 0.2 - 2\frac{(n_O - 3n_N)n_C}{(n_C + n_O - 3n_N)} \times 0.9 - n_N \times 2.5, \quad (2)$$

   where n_C, n_O, n_N, and n_H are the number of carbon, oxygen, nitrogen, and hydrogen atoms of the compound, respectively.

2. a parameterization based on HOM from α-pinene ozonolysis by Peräkylä et al. (2020) (scenario 2b):

$$\log_{10}(C) = n_C \times 0.18 - n_H \times 0.14 - n_O \times 0.38 + n_N \times 0.80 + 3.1, \quad (3)$$

   with similar parameter notation.

2.5 Simulations of the $RO_2^\bullet$ loss pathway based on the Master Chemical Mechanism (MCM)

The $RO_2^\bullet$ loss pathways were estimated based on MCM simulations (http://mcm.york.ac.uk/, last access: 14 November 2021). The gas-phase reactions of limonene +NO_3 under dark condition were simulated using iChamber, an open-source program (https://sites.google.com/view/wangsiyuan/models?authuser=0, last access: 14 November 2021) (Wang and Pratt, 2017). The default chemistry of limonene +NO_3 in the MCM was applied in this study (Saunders et al., 2003). Photolysis reactions were excluded by setting the zenith angle to 90°. Concentrations of O_3, NO_3, NO_2 and N_2O_5, and temperature and relative humidity were constrained to the experimental data with a time resolution of 1 min. The chamber dilution rate of $1.5 \times 10^{-5}\ s^{-1}$ was applied to all species. The P1 period was simulated using the above conditions, and the initial concentrations of limonene were added in the model according to the experimental procedures. The sum of all 140 $RO_2^\bullet$ in the limonene subset of MCM v3.3.1 were used

in the usual way to estimate the loss rates of $RO_2^\bullet$ bimolecular reactions. The reaction rate constants are provided in Table S3 in the Supplement, and calculated loss rates are shown in Fig. S3. We note that the MCM reaction schemes do not include the accretion reactions between HOM-$RO_2^\bullet$. Berndt et al. (2018a) determined the rate constant of accretion reaction of $C_{10}H_{15}O_4^\bullet$ formed via α-pinene ozonolysis to be $\sim 1 \times 10^{-11}$ cm^3 molecule^{-1} s^{-1}, which is of the same order as the upper limit for $RO_2^\bullet + RO_2^\bullet$ reactions used in the MCM schemes for functionalized peroxy radicals such as acyl peroxy radicals (Jenkin et al., 1997; Saunders et al., 2003). However, currently we do not see a reliable updated set of rate coefficients that are applicable to the reaction system in this study. If the rate constants of some $RO_2^\bullet + RO_2^\bullet$ reactions were higher than those used in MCM, the concentrations of $RO_2^\bullet$ would be lower and relative importance of $RO_2^\bullet + RO_2^\bullet$ in $RO_2^\bullet$ fate would increase. Several simulation results are shown in Fig. S4, including NO_3, N_2O_5, limonene, $RO_2^\bullet$, reaction rate of limonene with NO_3 ($k \times$ limonene $\times$ NO_3), and examples of first- and second-generation $RO_2^\bullet$.

In the early stage of each period, $RO_2^\bullet$ mainly reacted with $RO_2^\bullet$ and NO_3, although in the later stage the reaction with NO_2 also contributed to a significant fraction of $RO_2^\bullet$ loss (Fig. S3, showing period P1 as an example). During the period P1a which our peak assignment was based on, the $RO_2^\bullet$ loss was dominated by $RO_2^\bullet + RO_2^\bullet$ and $RO_2^\bullet + NO_3$.

3 Results and discussion

3.1 Experiment overview and observed HOM

After each limonene addition, the concentration of limonene rose first and then rapidly declined, while the concentrations of NO_3 and N_2O_5 rapidly decreased due to the fast reaction between limonene and NO_3, and gradually increased when limonene had been consumed (Fig. 1a). About 10 min after the first limonene addition, new particles had already formed and quickly grew in size (Fig. 1b). Therefore, we used the first 10 min reaction time (period P1a) to identify gas-phase HOM products, and the whole experiment to examine the contribution of HOM to SOA.

During period P1, HOM were quickly formed. We identified about 280 HOM compounds, including monomers (C_7-C_{10}, $\sim$280–460 Th), dimers (C_{17}-C_{20}, $\sim$490–700 Th), and trimers (C_{26}-C_{30}, $\sim$720–960 Th) (Fig. 2a). Their detailed formulas can be found in Table S1. HOM on the horizontal lines of the Kendrick mass defect plot (O-based) (Figs. 3, S5, and S6) share the same number of C, N, and H atoms, with the number of oxygen atoms increasing from left to right. Such HOM compounds are defined as a family. We notice that most monomer peroxy radical families are each related to two monomer closed-shell product families, with one H atom more or one H atom less, which are the expected termination products of $RO_2^\bullet + RO_2^\bullet$ reactions, or if $HO_2^\bullet$ is present, $RO_2^\bullet + HO_2^\bullet$ termination products. These three related families are defined as a "series", with the same number of C and N number, such as $C_{10}H_{15-17}NO_{6-14}$. In total, we identified 6 monomer series ($C_{10}H_{15-17}NO_{6-14}$, $C_{10}H_{14-16}N_2O_{9-15}$, $C_{10}H_{14-16}O_{7-12}$, $C_9H_{13-15}NO_{7-14}$, $C_8H_{11-13}NO_{6-13}$, and $C_7H_{9-11}NO_{7-11}$) and 1 monomer family ($C_{10}H_{17}N_3O_{12-16}$), 11 dimer families ($C_{20}H_{31}NO_{10-15}$, $C_{20}H_{33}NO_{12-16}$, $C_{20}H_{32}N_2O_{9-20}$, $C_{20}H_{31}N_3O_{14-20}$, $C_{20}H_{33}N_3O_{12-20}$, $C_{20}H_{34}N_4O_{15-20}$, $C_{20}H_{32}O_{13-16}$, $C_{19}H_{29}NO_{10-13}$, $C_{19}H_{31}NO_{10-15}$, $C_{19}H_{30}N_2O_{10-18}$, and $C_{19}H_{31}N_3O_{15-19}$), and 3 trimer families ($C_{30}H_{47}N_3O_{18-24}$, $C_{30}H_{48}N_4O_{16-24}$, and $C_{29}H_{46}N_4O_{19-24}$). The monomer family $C_{10}H_{17}N_3O_{12-16}$ is not classified as series because the supposedly relevant families are not clearly identified. Compounds containing at least one nitrogen atom accounted for more than 90 % of the identified HOM products. We assume that compounds containing nitrogen atoms are organic nitrates, because other N-containing species such as amines or nitro compounds are very unlikely to be formed from the reaction of limonene with NO_3. Organic nitrates formed in this study could be alkylnitrates, or (acyl)peroxynitrates formed via the reaction of $RO_2^\bullet$ with NO_2.

During period P1a, in the absence of particles, both HOM monomers and oligomers were observed, including monomers (47 %), dimers (47 %), and trimers (6 %) (Fig. 2a). Concentrations of gas-phase dimers and trimers decreased evidently after particle formation (Figs. 2b, 5, 6), indicating a fast gas–particle condensation and strong tendency of oligomers to condense on particles.

Based on their typical time series (Fig. 1c), products can be classified as first-generation or second-generation products. Generally, the concentrations of first-generation products, which result from the direct reaction of limonene with NO_3, are expected to quickly increase after the limonene addition, followed by a steady decline due to wall loss or chemical reactions. Concentrations of typical second-generation products, which result from further reactions of first-generation products, are expected to show a gradually increasing concentration pattern after a limonene addition and reach their maximum concentration later than first-generation products. These general expectations are modified in our case, since the particle concentration increased in our experiment (Fig. 1b) and the condensational sink of HOM products became stronger over time. Thus, an increase in concentration suggests that the increasing condensational sink was exceeded by increasing production with time, i.e., from second-generation pathways.

To sum up, gas-phase HOM formed in the limonene + NO_3 system were dominated by HOM monomers and dimers. Time series patterns of the products indicate multiple generations of reaction pathways.

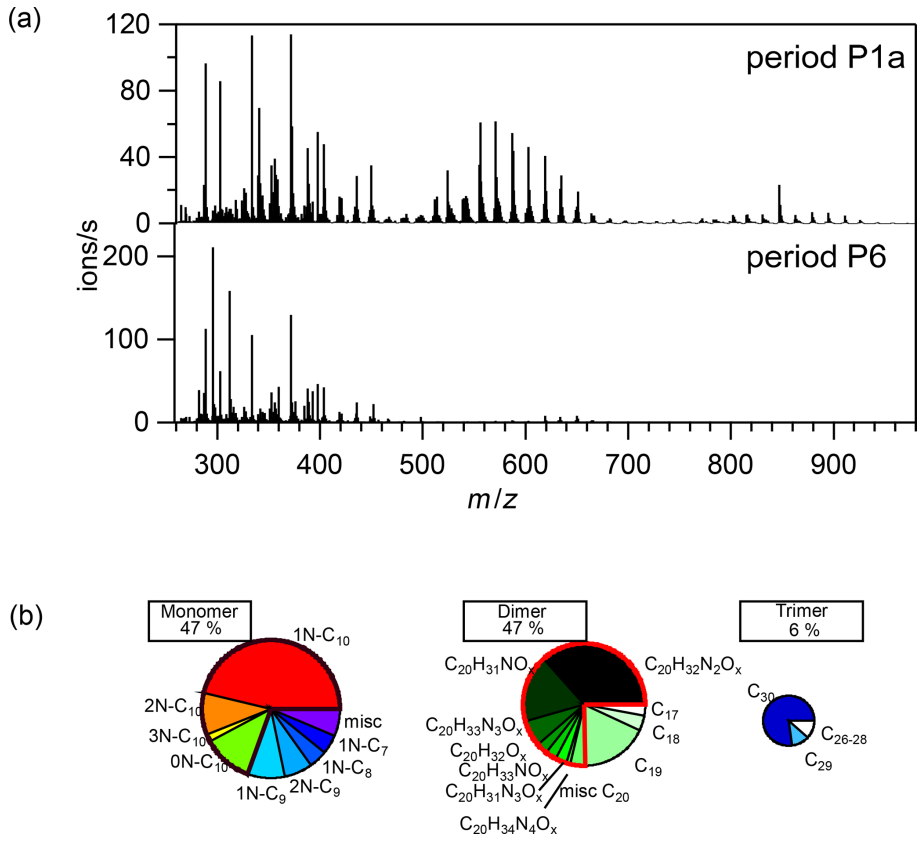

Figure 2. **(a)** Average mass spectra of the first 10 min reaction time after the first addition of limonene (period P1a, upper panel) and the last limonene addition period till particles reached maximum mass concentration (period P6, lower panel). **(b)** Pie charts (from left to right: rainbow, green, and blue colors) representing the relative contributions of identified families to HOM monomers, dimers, and trimers, respectively, during the P1a period. The area of each pie is in proportion to their concentrations during the P1a period.

3.2 Monomers and their formation pathways

3.2.1 Overview of HOM monomers

A number of HOM monomer families were detected with an increasing oxygenation pattern at 16 Th intervals (Fig. 3). Such a pattern is attributed to autoxidation of $RO_2^{\bullet}$ (with 32 Th interval for each O_2 addition) plus the alkoxy–peroxy pathway (shifted by 16 Th compared with exclusive autoxidation) as discussed below. During period P1a, the most abundant HOM monomers are C_{10} compounds (64 %), such as peroxy radicals $C_{10}H_{16}NO_x^{\bullet}$ and closed-shell products $C_{10}H_{15}NO_x$ and $C_{10}H_{17}NO_x$, which are carbonyl compounds and hydroxyl or hydroperoxy compounds from the termination reactions of $C_{10}H_{16}NO_x^{\bullet}$, respectively. Reaction (R14):

$$C_{10}H_{16}NO_x^{\bullet} + C_{10}H_{16}NO_x^{\bullet} \rightarrow C_{10}H_{15}NO_x + C_{10}H_{17}NO_x. \quad \text{(R14)}$$

According to the nitrogen atoms contained, C_{10}-HOM monomers can be classified into 1N-, 2N-, 3N-monomers, and monomers without nitrogen atoms. While 1N-C_{10} HOM monomers were likely formed by direct NO_3 addition to limonene, C_{10} HOM monomers containing multiple N atoms were likely formed via multiple reaction steps. Besides C_{10} HOM monomers, C_{6-9} HOM monomers were also observed. These C_{6-10} families are discussed below in the order of their contributions to HOM monomers.

3.2.2 1N-C_{10} monomers

Among C_{10} HOM monomers, the 1N-C_{10} families were most abundant and included stable closed-shell products $C_{10}H_{15}NO_x$ ($x = 7$–13) and $C_{10}H_{17}NO_x$ ($x = 9$–14) and peroxy radicals $C_{10}H_{16}NO_x^{\bullet}$ ($x = 6$–14). The concentration of $C_{10}H_{16}NO_{11}^{\bullet}$ increased in the later phase of each limonene addition period (Fig. 1c), showing mostly a time profile of a second-generation product, similar as most of the other radicals in the $C_{10}H_{16}NO_x^{\bullet}$ family (Fig. S7). However, the time series of $C_{10}H_{15}NO_x$ compounds showed an overlaying pattern of first- and second-generation products dominated by a second-generation time profile with the exception of $C_{10}H_{15}NO_9$ (Fig. 1c). Due to sensitivity restrictions of CIMS, the primary peroxy radical $C_{10}H_{16}NO_5^{\bullet}$ was not detected, which was supposed to show first-generation pattern.

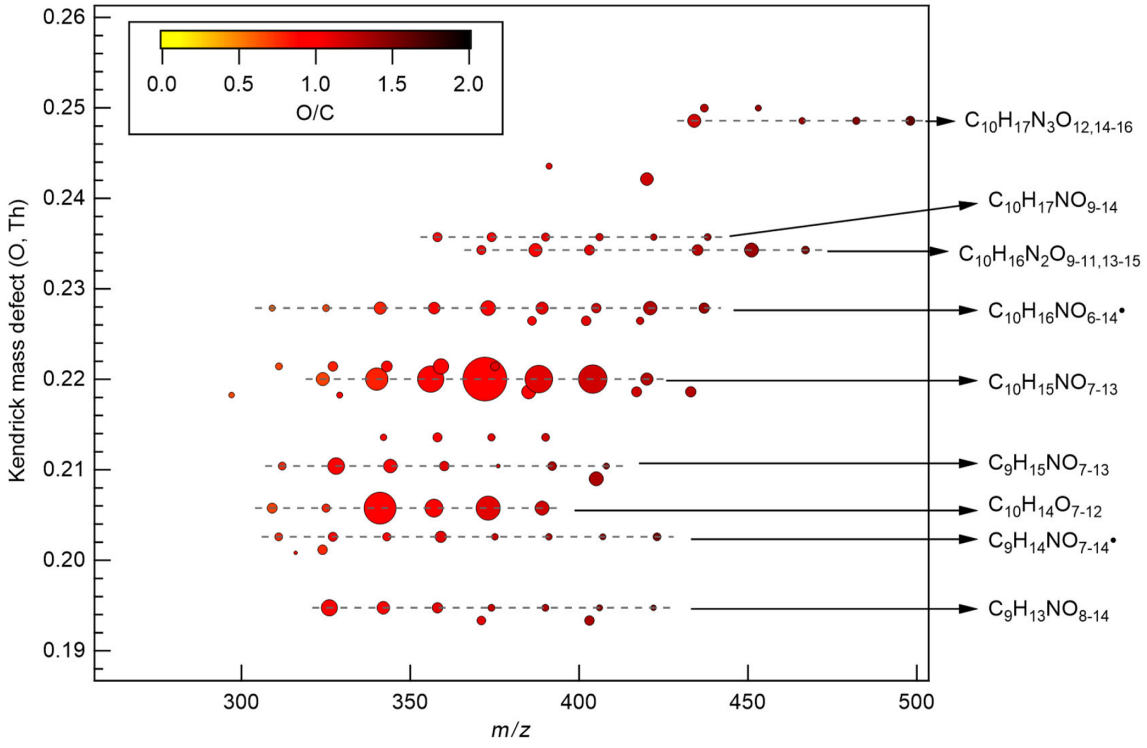

Figure 3. Kendrick mass defect plot (O-atom-based) of major monomer products. The area of the circles is proportional to the average intensity of each compound during the P1a period with the largest circle representing $C_{10}H_{15}NO_{10}$. The color denotes O/C ratios. Dashed lines indicate major product families. For clarity, the reagent ions $^{15}NO_3^-$ are omitted from molecular formula. The calculation of O-atom-based Kendrick mass defect includes two steps. First, the IUPAC mass scale (based on the ^{12}C atomic mass as exactly 12 Da) is rescaled to Kendrick mass: Kendrick mass = IUPAC mass $\times(16/15.9949)$, which converts the mass of O from 15.9949 to exactly 16. Then, Kendrick mass defect is given by Kendrick mass defect = nominal Kendrick mass − exact Kendrick mass. Thus, compounds with the same number of each kind of atom except for O have equal O-atom-based Kendrick mass defect, and are shown in a horizontal line in the O-atom-based Kendrick mass defect plot.

The absence of first-generation characteristics of the time profile of most HOM peroxy radicals $C_{10}H_{16}NO_x^{\bullet}$ ($x \geq 6$) may be attributed to two possible reasons. They either did not undergo efficient autoxidation, or they underwent immediate conversion including autoxidation and/or bimolecular reactions with other $RO_2^{\bullet}$ or NO_3 forming closed-shell products such as dimers or continuing the radical chain forming $RO^{\bullet}$. The instantaneous increase of 2N-dimers and trimers after the first limonene addition shown below suggests that $C_{10}H_{16}NO_x^{\bullet}$ ($x \geq 6$) were indeed formed efficiently via autoxidation. Therefore, the latter reason is more likely. At this time, we do not have a reasonable explanation for the trend of $C_{10}H_{15}NO_9$, though we should consider that there are many isomers at play, which may have very different chemical pathways (un)available.

Since the $C_{10}H_{15}NO_x$ family showed an overlaying pattern of the first-generation and second-generation products, they likely contained multiple isobaric substances produced through different pathways. Based on the literature, possible formation pathways of these products were tentatively proposed (Seinfeld and Pandis, 2006; Vereecken and Peeters, 2010; Mentel et al., 2015; Vereecken and Nozière, 2020). As an example of the pathways to form first-generation products, $C_{10}H_{16}NO_{2x-1}^{\bullet}$ (with an odd number of oxygen atom) and their corresponding termination products can be formed via autoxidation of the first peroxy radical $C_{10}H_{16}NO_5^{\bullet}$ (R1OO), showing $C_{10}H_{16}NO_9^{\bullet}$ (R3OO) as an example (scheme 1a, first-generation products). $C_{10}H_{16}NO_{2x}^{\bullet}$ (with an even number of oxygen atom) can be formed via alkoxy–peroxy channels. For example, the ring-opening of the alkoxy radical $C_{10}H_{16}NO_4^{\bullet}$ (R1O), which was formed via the reaction of $C_{10}H_{16}NO_5^{\bullet}$ (R1OO) with another $RO_2^{\bullet}$ or NO_3 radical (scheme 1a, first-generation products). Ring-opening of R1O leads to $C_{10}H_{16}NO_6^{\bullet}$ (R4OO), which can undergo autoxidation forming $C_{10}H_{16}NO_{2x}^{\bullet}$. In addition, the alkoxy radical $C_{10}H_{16}NO_4^{\bullet}$ (R1O) is susceptible to ring-opening reactions (Novelli et al., 2021), which can lead to a first-generation stable product 3-isopropenyl-6-oxoheptanal (endolim, TP1) after C-C bond cleavage followed by the elimination of a NO_2 fragment (scheme 1b, second-generation products). Endolim (TP1) has been detected as a major product in previ-

ous limonene $+NO_3$ studies (Hallquist et al., 1999; Spittler et al., 2006).

As an example of second-generation chemistry, the remaining double bond of endolim could react with NO_3 to form $RO_2^{\bullet}$, followed by the autoxidation to form second-generation $C_{10}H_{16}NO_x^{\bullet}$ (with odd number of oxygen atoms). Similar to first-generation pathways, second-generation $C_{10}H_{16}NO_x^{\bullet}$ with even number of oxygen atoms can be formed via alkoxy–peroxy channel. From the time profile of $C_{10}H_{15}NO_x$, the second-generation pathway (scheme 1b) was expected to play a more important role, in agreement with the theoretical result by Kurtén et al. (2017), in which the two bond–cleavage pathways of limonene-derived $RO^{\bullet}$ radical were considered. It is worth mentioning that the reaction products of limonene with O_3 may also react with NO_3, forming $C_{10}H_{16}NO_x^{\bullet}$ (scheme S1). However, as shown above, this was a minor pathway in our experiment (Sect. 2.1). We would like to note that to simplify the scheme, only the reaction of NO_3 with the endocyclic double bond is presented, since this reaction is faster than that with the exocyclic double bond (Jiang et al., 2009; Fry et al., 2011).

$C_{10}H_{16}NO_x^{\bullet}$ with both even and odd number of oxygen atoms and their termination products had comparable abundance, which suggests that the alkoxy–peroxy pathway was important for $RO_2^{\bullet}$ formation in this reaction. This finding is analogous to the findings in the reaction of a number of alkenes with O_3 and in the reaction of isoprene and β-pinene with NO_3 (Mentel et al., 2015; Zhao et al., 2021; Shen et al., 2021).

Among 1N-C_{10} monomers, concentrations of carbonyl compounds were much higher than the sum of hydroxy- and hydroperoxy-substituted compounds (Table 1). According to Hyttinen et al. (2015), for nitrate CI-APi-TOF, HOM containing two hydrogen bond donors (such as -OOH and -OH group) have strong binding energy with NO_3^-. Additional hydrogen bond donors only enhance the binding energy marginally. If we compare HOM carbonyl product (such as $C_{10}H_{15}NO_{10}$) with the corresponding hydroxy product ($C_{10}H_{17}NO_{10}$), they only differ in one functional group. As both are highly functionalized, it is likely that HOM carbonyl have a quite similar sensitivity with HOM alcohol. If the sensitivity of carbonyl HOM were lower, this would result in even more dominance of carbonyl HOM over hydroxyl HOM. Thus, we conclude that carbonylnitrates are more abundant than hydroxynitrates or hydroperoxynitrates. This finding is likely attributed to unimolecular termination reactions of $RO_2^{\bullet}$, although reaction paths via $RO^{\bullet}$ also cannot be excluded. Smaller unbranched $RO^{\bullet}$ tend to react with O_2 forming carbonyl compounds, while for larger or branched $RO^{\bullet}$, isomerization can also form carbonyl compounds and is a more energetically favorable and thus faster pathway compared with the reaction with O_2 (Ziemann and Atkinson, 2012). The importance of unimolecular termination reactions of HOM-$RO_2^{\bullet}$ and the resulting high ratio of carbonyl compounds to hydroxyl/hydroperoxyl compounds has also been found in the reaction system of β-pinene $+NO_3$ (Shen et al., 2021; Dam et al., 2022). This high ratio is also consistent with findings in the ozonolysis of alkenes (Mentel et al., 2015), where unimolecular termination reactions were also proposed to be the likely explanation (Crounse et al., 2013; Rissanen et al., 2014). As discussed in our previous study by Shen et al. (2021), this higher abundance of carbonylnitrates is not likely to be explained by the reaction of alkoxy $RO^{\bullet} + O_2$ forming carbonyls and $HO_2^{\bullet}$, decomposition of β-nitrooxyperoxynitrate, or self-reactions of $RO_2^{\bullet}$ via the Bennett and Summers mechanism forming carbonyls and H_2O_2. Reactions between $RO_2^{\bullet}$ in general should produce overall equal amounts of carbonyl and hydroxyl compounds. The decomposition of β-nitrooxyperoxynitrate is slow in the gas-phase. The reaction of alkoxy $RO^{\bullet}$ with O_2 for large $RO^{\bullet}$ is generally slower than isomerization and decomposition (Vereecken and Peeters, 2009, 2010). Thus, the higher abundance of carbonylnitrates compared to hydroxynitrates may be attributed to unimolecular termination of HOM-$RO_2^{\bullet}$. In addition, isomerization of $RO^{\bullet}$ forming carbonyl compounds may also contribute to this finding. Our result thus further emphasizes that unimolecular termination reactions of RO_2 radicals are important pathways in the formation of HOM monomers derived from the reactions of monoterpenes with NO_3 (Shen et al., 2021). Scheme 1c shows this unimolecular termination process using a $C_{10}H_{16}NO_9^{\bullet}$ radical as an example. $C_{10}H_{16}NO_9^{\bullet}$ undergoes a 1,4-H-shift, and O_2 addition to form a $C_{10}H_{16}NO_{11}^{\bullet}$ radical. The $C_{10}H_{16}NO_{11}^{\bullet}$ radical further undergoes an H-shift of the α-OOH H-atom, which produces a carbonyl closed-shell product and an $OH^{\bullet}$ radical.

For 1N-C_{10} HOM monomers, the products detected in this study generally agree with previous laboratory and field studies on the reaction of limonene and other monoterpenes. Faxon et al. (2018) also observed $C_{10}H_{15}NO_x$ as the most prevalent products in the particle phase from limonene $+NO_3$. In the SOAS campaign, both $C_{10}H_{15}NO_x$ and $C_{10}H_{17}NO_x$ products were detected and were believed to be products of nighttime chemistry (Lee et al., 2016). The high abundance of 1N-C_{10} HOM monomers is consistent with the finding that $C_{10}H_{15}NO_x$ and $C_{10}H_{17}NO_x$ dominate the chemical composition of SOA formed via NO_3 oxidation of α-pinene and β-pinene, as shown in previous chamber studies (Takeuchi and Ng, 2019).

In summary, 1N-C_{10} HOM monomers are mainly formed via second-generation pathways, and unimolecular termination of $RO_2^{\bullet}$ likely plays an important role leading to higher abundance of carbonyl HOM-ON ($C_{10}H_{15}NO_x$) than hydroxy/hydroperoxy HOM-ON ($C_{10}H_{17}NO_x$).

3.2.3 2N and 3N-C_{10} monomers

C_{10} monomers with 2 and 3 nitrogen atoms accounted for 27 % and 1 % of HOM monomers, respectively. They were likely formed via the reaction of a second attack

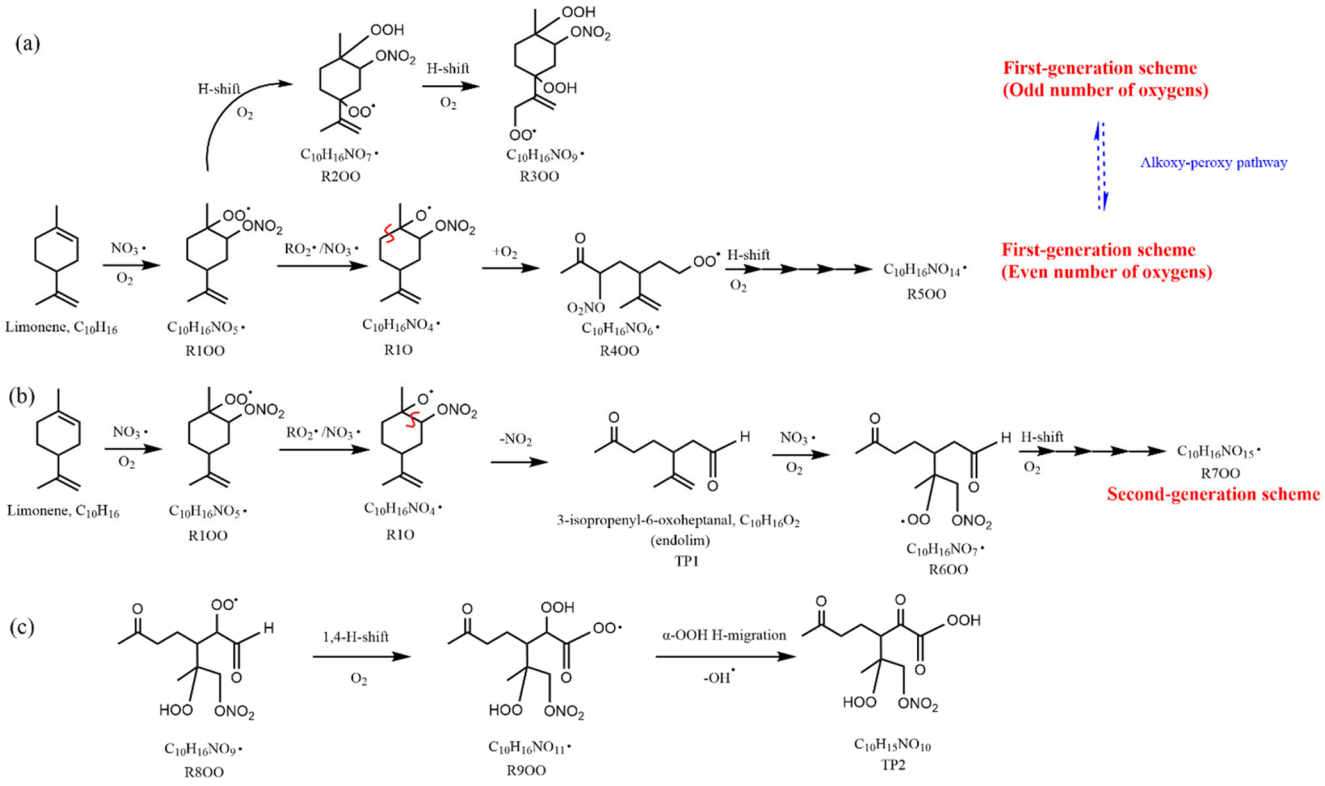

Scheme 1. Illustrative scheme for HOM formation in the limonene $+NO_3$ reaction. **(a)** Example formation pathways leading to first-generation 1N-C_{10} HOM-RO_2 radicals ($C_{10}H_{16}NO_x^{\bullet}$ with even or odd numbers of O-atoms). **(b)** Second-generation scheme involving the formation of endolim. **(c)** Scheme of intramolecular termination of $RO_2^{\bullet}$ radicals forming carbonyl products taking the $C_{10}H_{16}NO_9^{\bullet}$ radical as an example. Note that the depicted reactions may not be the dominant pathways.

of NO_3 to the first-generation products as the 1N-C_{10} closed-shell products formed via the reactions shown in scheme 1a should contain a remaining limonene C=C double bond. Typical 2N- and 3N-HOM showed a second-generation time profile (Fig. 4). For clarity, only periods P1 to P3 are shown. This time profile is consistent with the pathways with multiple NO_3 attacks. Scheme 2 shows possible formation pathways of 2N- and 3N-C_{10} monomers. 2N-C_{10} HOM were likely to be formed from NO_3 oxidation of 1N-C_{10} monomers ($C_{10}H_{15}NO_x$ and $C_{10}H_{17}NO_x$), resulting in $C_{10}H_{15}N_2O_x^{\bullet}$ and $C_{10}H_{17}N_2O_x^{\bullet}$ (scheme 2a, b). While $C_{10}H_{15}N_2O_x^{\bullet}$ ($x = 9$–12) were observed, $C_{10}H_{17}N_2O_x^{\bullet}$ could not be uniquely identified because the peaks of the $C_{10}H_{17}N_2O_x^{\bullet}$ and $C_{10}H_{15}NO_x$ families are too close in the mass spectra to be separated based on the resolution of our mass spectrometer. 3N-C_{10} monomers, $C_{10}H_{17}N_3O_x$, were expected to be formed from limonene via two steps of NO_3 oxidation to the double bonds and an addition of NO_2 to an RO_2 radical, leading to a peroxynitrate or peroxyacylnitrate. NO_2 addition reactions may also contribute to the formation of 2N-C_{10} monomers. The addition of NO_2 to RO_2 radicals could occur either before (scheme 2d) or after (scheme 2c) the second NO_3 attack.

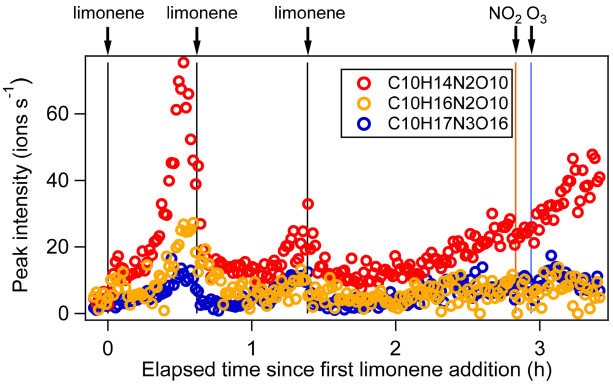

Figure 4. Time series of peak intensity of several monomers $C_{10}H_{14}N_2O_{10}$, $C_{10}H_{16}N_2O_{10}$, and $C_{10}H_{17}N_3O_{16}$ as the representatives of multiple N monomers during the periods P1 to P3.

3.2.4 Formation pathways of C_{10} monomers without N-atoms and monomers with less than 10 C-atoms

Besides C_{10} products containing nitrogen atoms, HOM monomers without nitrogen atoms were also identified. Among these products, $C_{10}H_{14}O_x$ ($x = 7$–12) were the most

Table 1. Observed $C_{10}H_{16}NO_x^{\bullet}$ radicals (m) and their termination products, including carbonyl compounds (m−17), hydroxyl compounds (m−15), and hydroperoxy compounds (m+1). Their concentrations during period P1a are normalized to that of $C_{10}H_{15}NO_{10}$, which had the highest concentration among the families of 1N-C_{10} monomers. Their relative signal intensities during the P1a period are shown in the second line of each cell.

Peroxy radical m	Carbonyl m−17	Hydroxy m−15	Hydroperoxy m+1
$C_{10}H_{16}NO_6^{\bullet}$ 1.5 %			
$C_{10}H_{16}NO_7^{\bullet}$ 2.0 %			
$C_{10}H_{16}NO_8^{\bullet}$ 6.7 %	$C_{10}H_{15}NO_7$ 8.0 %		
$C_{10}H_{16}NO_9^{\bullet}$ 6.0 %	$C_{10}H_{15}NO_8$ 25.2 %		$C_{10}H_{17}NO_9$ 3.7 %
$C_{10}H_{16}NO_{10}^{\bullet}$ 10.2 %	$C_{10}H_{15}NO_9$ 34.6 %	$C_{10}H_{17}NO_9$ 3.7 %	$C_{10}H_{17}NO_{10}$ 3.6 %
$C_{10}H_{16}NO_{11}^{\bullet}$ 6.6 %	$C_{10}H_{15}NO_{10}$ 100.0 %	$C_{10}H_{17}NO_{10}$ 3.6 %	$C_{10}H_{17}NO_{11}$ 3.0 %
$C_{10}H_{16}NO_{12}^{\bullet}$ 4.1 %	$C_{10}H_{15}NO_{11}$ 39.0 %	$C_{10}H_{17}NO_{11}$ 3.0 %	$C_{10}H_{17}NO_{12}$ 2.3 %
	$C_{10}H_{15}NO_{12}$ 41.2 %	$C_{10}H_{17}NO_{12}$ 2.3 %	$C_{10}H_{17}NO_{13}$ 1.5 %
$C_{10}H_{16}NO_{14}^{\bullet}$ 4.7 %	$C_{10}H_{15}NO_{13}$ 6.7 %	$C_{10}H_{17}NO_{13}$ 1.5 %	$C_{10}H_{17}NO_{14}$ 1.8 %
		$C_{10}H_{17}NO_{14}$ 1.8 %	

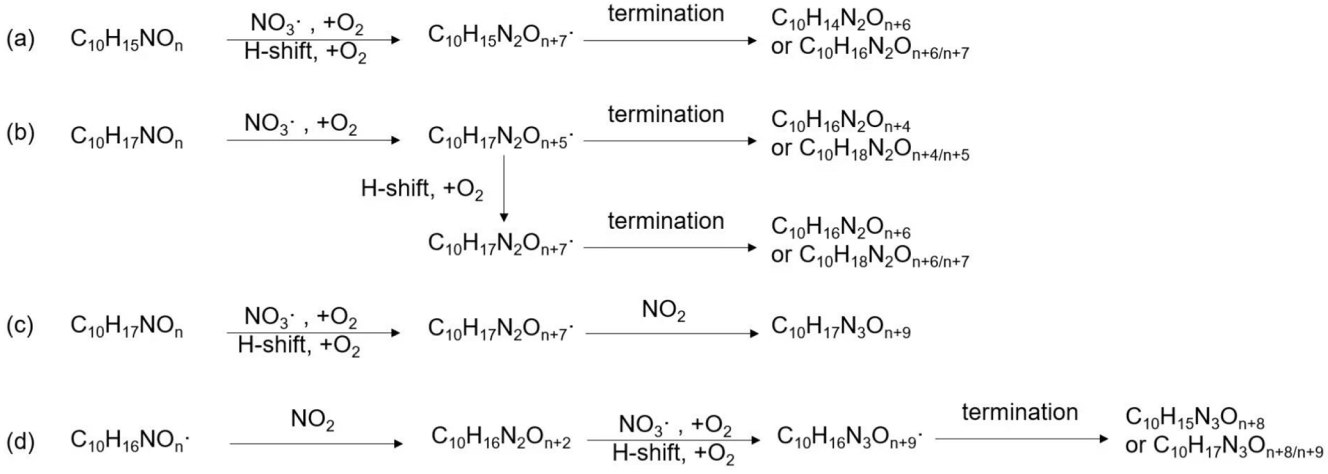

Scheme 2. Possible formation pathways of C_{10}-monomers containing 2 nitrogen atoms **(a, b)** and 3 nitrogen atoms **(c, d)**. Termination denotes reactions of $RO_2^{\bullet}$ with other $RO_2^{\bullet}$ or HO_2, or unimolecular reactions, leading to closed-shell products.

prevalent family, which were also detected in limonene ozonolysis (Jokinen et al., 2015). The $C_{10}H_{14}O_x$ family showed a time series typical of first-generation products (Fig. S8). $C_{10}H_{14}O_x$ and $C_{10}H_{16}O_x$ could be formed from limonene $+NO_3$ with $C_{10}H_{16}NO_x^{\bullet}$ terminating their autoxidation by migration of the α-NO_3 H-atom, eliminating an NO_2 fragment (scheme S2) (Novelli et al., 2021). Alternatively, these products could be formed via the reaction of O_3 with limonene (scheme S2). Either way, $C_{10}H_{14}O_x$ and $C_{10}H_{16}O_x$ were formed via first-generation pathways.

We also observed monomers with carbon atom number less than 10. During the P1a period, C_9 monomer families were the most abundant contributors to $C < 10$ HOM monomers, followed by C_8 families. The majority of C_9 monomers were $C_9H_{15}NO_x$ ($x = 7$–13) (time series shown in Fig. S9) and $C_9H_{13}NO_x$ ($x = 8$–14). The loss of one carbon atom may follow the mechanism shown in scheme S3 (Fry et al., 2011; Bianchi et al., 2019). The major product family in C_8 monomers is $C_8H_{11}NO_x$ ($x = 6$, 7, 9–13). While during period P1a $C_8H_{11}NO_x$ compounds could be hardly observed, their concentrations increased considerably in the later periods (Fig. S10). The gas-phase concentration of $C_8H_{11}NO_7$ was even the highest among all compounds in later periods (highest intensity signal in Fig. 2b). This is partly attributed to the relatively high volatility of C_8 compounds compared with C_{10} HOM species and accretion products, which tend to condense on particles. The major family in C_7 monomers, $C_7H_9NO_x$ ($x = 6$–13), showed a time series pattern similar to $C_8H_{11}NO_x$ compounds (Fig. S11). Such a time profile indicates that C_7 and C_8 products were likely a result of multi-generation gas-phase reactions.

3.3 Dimers and their formation

Among dimers, C_{20} products were the most abundant, followed by C_{19} products. Among C_{20} and C_{19} dimers, the most prevalent families included $C_{20}H_{32}N_2O_x$ ($x = 9$–20), $C_{20}H_{33}N_3O_x$ ($x = 12$–20), $C_{20}H_{31}NO_x$ ($x = 10$–15), $C_{20}H_{31}N_3O_x$ ($x = 14$–20), $C_{20}H_{34}N_4O_x$ ($x = 15$–20), and $C_{19}H_{30}N_2O_x$ ($x = 10$–18) (Fig. S5). The O/C ratio of dimers did not exceed one, while that of monomers was as high as two. This could be due to oxygen atom loss and participation of less oxygenated $RO_2^{\bullet}$ in the dimer formation as discussed below. Time series of dimers also showed different behavior compared to monomers. For example, compounds of the $C_{20}H_{32}N_2O_x$ family only reached a considerable peak intensity in period P1 and decreased rapidly thereafter, while the signal intensity in periods P2 to P6 were low (Fig. 5). Generally, other dimers showed similar patterns (Figs. S12–S14), though the difference of their concentration between P2-P6 and P1 were not as large as for the $C_{20}H_{32}N_2O_x$ family. The time when signals of several dimers (e.g., $C_{20}H_{32}N_2O_x$, $C_{20}H_{33}N_3O_x$, $C_{20}H_{34}N_4O_x$) dropped substantially matched the time of new particle formation (NPF) and the onset of particle growth, indicating that some dimers were likely involved in the early growth of particles. Such a behavior is expected since dimers have a much lower volatility than monomers. This observation is consistent with the limonene $+NO_3$ laboratory study by Faxon et al. (2018) that found a significant fraction of HOM dimer derived in the particle phase.

In general, $C_{20}H_{32}N_2O_x$ showed an overlaying time profile of first- and second-generation products (Fig. 5). $C_{20}H_{32}N_2O_x$ were likely formed via the accretion reaction between two monomer $RO_2^{\bullet}$ ($C_{10}H_{16}NO_x^{\bullet}$):

$$C_{10}H_{16}NO_{x1}^{\bullet} + C_{10}H_{16}NO_{x2}^{\bullet} \rightarrow C_{20}H_{32}N_2O_{x1+x2-2} + O_2. \quad \text{(R15)}$$

Since $C_{10}H_{16}NO_x^{\bullet}$ can be first- or second-generation products, the resulting dimers $C_{20}H_{32}N_2O_x$ can also be first- or second-generation products. The time series shows that $C_{20}H_{32}N_2O_x$ with lower O number presented more of a first-generation product time profile (Fig. 5), while the relative contribution of second-generation formation was observed to increase with oxygen number.

We compared the observed dimer formula with those expected based on accretion reactions of HOM-$RO_2^{\bullet}$. x in the $C_{20}H_{32}N_2O_x$ observed was ≥ 9; however, according to the accretion mechanism and the observed $C_{10}H_{16}NO_x^{\bullet}$ ($x \geq 6$), x in $C_{20}H_{32}N_2O_x$ should be ≥ 10 ($6+6-2=10$). Moreover, as the most abundant $RO_2^{\bullet}$ within the $C_{10}H_{16}NO_x^{\bullet}$ family was $C_{10}H_{16}NO_{10}^{\bullet}$ (Table 1), the most abundant $C_{20}H_{32}N_2O_x$ would have an oxygen number of 18 if they were exclusively formed by the accretion reaction of HOM $RO_2^{\bullet}$. This contradicted the fact that the most abundant molecule among the $C_{20}H_{32}N_2O_x$ family was $C_{20}H_{32}N_2O_{13}$. The findings above could only be explained by the participation of less oxygenated $RO_2^{\bullet}$ such as $C_{10}H_{16}NO_{5,6}^{\bullet}$ in the accretion reaction (Berndt et al., 2018a, b; McFiggans et al., 2019). $C_{10}H_{16}NO_5^{\bullet}$ was not detected by our CI-APi-TOF, which is attributed to the lower detection sensitivity of molecules with O number ≤ 5 in the NO_3^--CIMS (Riva et al., 2019). Still, $C_{10}H_{16}NO_5^{\bullet}$ is the first RO_2 radical formed in the limonene $+NO_3$ reaction (scheme 1a) so a high mass flux has to pass through this $RO_2^{\bullet}$. If we assume that the abundance of $C_{10}H_{16}NO_5^{\bullet}$ was high, and considering that the concentration of $C_{10}H_{16}NO_{10}^{\bullet}$ was the highest in the $C_{10}H_{16}NO_x^{\bullet}$ family, their accretion reaction (R16) could form $C_{20}H_{32}N_2O_{13}$ and support that $C_{20}H_{32}N_2O_{13}$ was the most abundant C_{20} dimer product:

$$C_{10}H_{16}NO_5^{\bullet} + C_{10}H_{16}NO_{10}^{\bullet} \rightarrow C_{20}H_{32}N_2O_{13} + O_2. \quad \text{(R16)}$$

Time series of dimers with different numbers of N atoms were different, indicating different formation pathways. For example, the $C_{20}H_{31}NO_x$ family were mainly first-generation products (Fig. S12), which may be formed via the following reaction:

$$C_{10}H_{16}NO_{x1}^{\bullet} + C_{10}H_{15}O_{x2}^{\bullet} \rightarrow C_{20}H_{31}NO_{x1+x2-2} + O_2. \quad \text{(R17)}$$

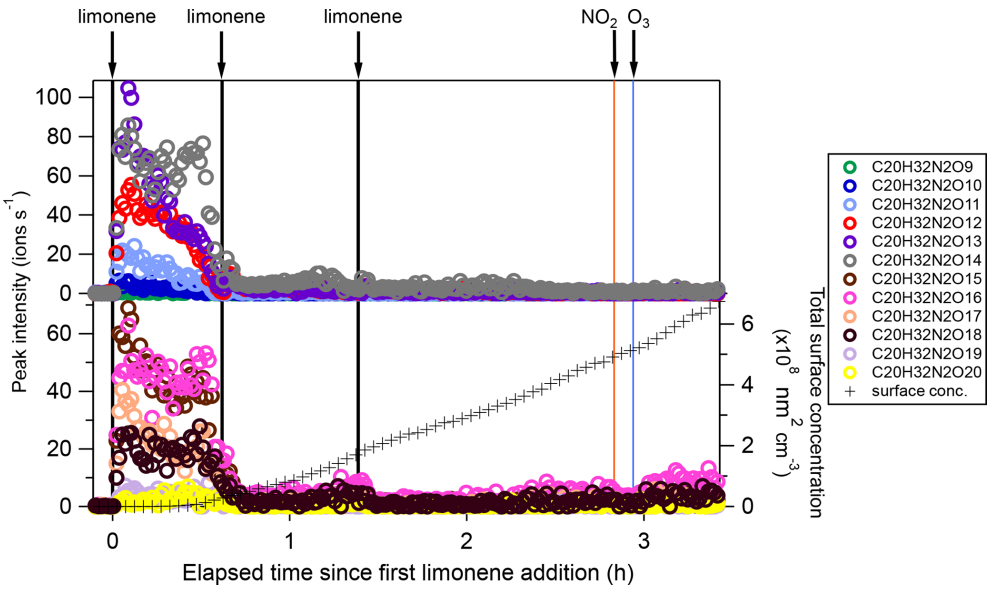

Figure 5. Time series of peak intensity of the $C_{20}H_{32}N_2O_x$ family compounds during the periods P1 to P3. The cross markers (lower right y axis) indicate total particle surface concentration.

$C_{10}H_{15}O_x^{\bullet}$ were first-generation radicals (Sect. 3.2.4), while $C_{10}H_{16}NO_x^{\bullet}$ were mainly second-generation radicals. $C_{10}H_{16}NO_x^{\bullet}$ could also be formed via first-generation pathway as discussed above (scheme 1a), but that was not borne out by the time profile, suggesting a fast termination of first-generation $C_{10}H_{16}NO_x^{\bullet}$ radicals. Reaction (R17) could be one of the termination pathways of first-generation $C_{10}H_{16}NO_x^{\bullet}$ based on the first-generation time profile of $C_{20}H_{31}NO_x$. In the study by Faxon et al. (2018), the formation of 1N-C_{20} dimers was explained by a mechanism involving two 1N-RO_2 radicals which produced HNO_3 as a by-product. However, C_{10} RO_2 radicals without nitrogen atoms were identified in our study, which provided a direct formation pathway of 1N-C_{20} dimers through reaction (R17).

On the other hand, $C_{20}H_{33}N_3O_x$ and $C_{20}H_{34}N_4O_x$ were mainly second-generation products (Figs. S13, S14). $C_{20}H_{33}N_3O_x$ and $C_{20}H_{34}N_4O_x$ were likely to be formed via NO_3 oxidation of dimers containing less nitrogen atoms, and were thus second-generation products. The related radicals were also detected, such as $C_{20}H_{32}N_3O_x^{\bullet}$ ($x = 16$–19) and $C_{20}H_{31}N_2O_x^{\bullet}$ ($x = 13$–16). Possible formation pathways of dominant oligomer families are displayed in Table 2. We cannot exclude that the formation pathway of $C_{20}H_{33}NO_x$, $C_{20}H_{34}N_4O_x$, and $C_{19}H_{31}NO_x$ may also involve limonene oxidation by $OH^{\bullet}$ (Table 2), which can be formed in the ozonolysis of limonene as a minor pathway. In addition, the high abundance of $C_{20}H_{31}NO_x$ ($x = 10$–15) among the dimers may be partly attributed to a contribution of the reaction of limonene with O_3.

The initial drop of the products (dimers and monomers) in Figs. 1, S8, and S12 during P1 (the characteristic time of the fastest decay was 15, 10, and 13 min, respectively) is attributed to the balance of their sources via the reaction of limonene with NO_3, their wall loss, and their potential loss by the reaction with NO_3. The characteristic time of the fastest decay of the HOM over the second limonene addition in Figs. 1, 4, 5, S12, and S13 are 4–8 min. These decays can be explained by the wall loss rate (characteristic time $\sim$ 8 min) and condensation sink of vapor loss to particles according to the study of Kulmala et al. (2012) (characteristic time $\sim$ 13 min). The characteristic times of the fastest decay of the HOM at the end of P2 in Figs. S12 and S13 are 1.4–3.4 min, which can also be well explained by the updated wall loss rate and condensation sink of vapor loss to particles at the end of P2 (characteristic time $\sim$ 1.4 min). In addition, for some HOM (e.g., $C_{10}H_{15}NO_{10}$, Fig. 1; $C_{10}H_{14}N_2O_{10}$, Fig. 4; $C_{20}H_{33}N_3O_{17}$, Fig. S13; $C_{20}H_{34}N_4O_{17}$, Fig. S14), the times of limonene additions (except for the first time) matched the time when HOM signals dropped rapidly. This phenomenon implies a sudden decrease of the source of these HOM at limonene additions as sinks including the losses to walls and particles were largely invariant in such a short time. The decrease of the source may be attributed to the rapid depletion of NO_3 at limonene injections (Fig. 1). As many of these HOM are second-generation products, i.e., formed via the reactions of first-generation products with NO_3, the depletion of NO_3 could lead to sudden decreases of the source of the second-generation HOM, which accounted for most HOM in the study.

In summary, HOM dimers are likely to be formed via accretion reactions of monomer $RO_2^{\bullet}$, and some dimers can undergo secondary oxidation by NO_3. Some dimers were likely involved in the early growth of SOA particles.

Table 2. Major dimer and trimer families and their possible formation pathways.

Dimer/trimer family	Possible formation pathways
$C_{20}H_{32}N_2O_x$	$C_{10}H_{16}NO_x^{\bullet} + C_{10}H_{16}NO_x^{\bullet}$
$C_{20}H_{33}N_3O_x/C_{20}H_{31}N_3O_x$	$C_{20}H_{32}N_2O_x + NO_3 + HO_2^{\bullet}/RO_2^{\bullet}$
$C_{20}H_{31}NO_x$	$C_{10}H_{16}NO_x^{\bullet} + C_{10}H_{15}O_x^{\bullet}$
$C_{20}H_{33}NO_x$	$C_{10}H_{16} + OH^{\bullet} + C_{10}H_{16}NO_x^{\bullet}$
$C_{20}H_{34}N_4O_x$	$(C_{10}H_{16}N_2O_x + OH^{\bullet}) + (C_{10}H_{16}N_2O_x + OH^{\bullet})$
$C_{19}H_{30}N_2O_x$	$C_{10}H_{16}NO_x^{\bullet} + C_9H_{14}NO_x^{\bullet}$
$C_{19}H_{31}N_3O_x$	$C_{19}H_{30}N_2O_x + NO_3 + HO_2^{\bullet}/RO_2^{\bullet}$
$C_{19}H_{29}NO_x$	$C_9H_{14}NO_x^{\bullet} + C_{10}H_{15}O_x^{\bullet}$
$C_{19}H_{31}NO_x$	$C_{10}H_{16} + OH^{\bullet} + C_9H_{14}NO_x^{\bullet}$
$C_{30}H_{48}N_4O_x$	$C_{20}H_{32}N_3O_x^{\bullet} + C_{10}H_{16}NO_x^{\bullet}$
$C_{30}H_{47}N_3O_x$	$C_{20}H_{31}N_2O_x^{\bullet} + C_{10}H_{16}NO_x^{\bullet}$

3.4 Trimers and their formation

Trimers (C_{26-30}) were dominated by C_{30} compounds (Fig. S6, Table S1). To the best of our knowledge, this is the first study that identified gas-phase trimers in the limonene $+NO_3$ reaction. The O/C ratio of trimers was lower than that of monomers and dimers, suggesting possible multiple accretion reactions in their formation pathways, which lose 2 oxygen atoms in each reaction. As each accretion reaction terminates the peroxy radical chain, the observation of trimers also implies that some dimers could further react with NO_3, creating dimer $RO_2^{\bullet}$. The most prevalent product families were $C_{30}H_{48}N_4O_x$ ($x = 16$–24) and $C_{30}H_{47}N_3O_x$ ($x = 18$, 19, 21, 23, 24), which were likely formed via the most abundant monomer RO_2 radicals – $C_{10}H_{16}NO_x^{\bullet}$ and the most abundant dimer RO_2 radicals – $C_{20}H_{32}N_3O_x^{\bullet}$ and $C_{20}H_{31}N_2O_x^{\bullet}$. Trimers from other monoterpenes $+NO_3$ have been observed in previous laboratory studies. For example, $C_{30}H_{48}N_4O_{16}$ and $C_{30}H_{47}N_3O_{16}$ were observed in the mass spectra of α-pinene $+NO_3$ SOA by C. Wu et al. (2021), and $C_{30}H_{47}N_3O_{13}$ was identified in β-pinene $+NO_3$ SOA by Claflin and Ziemann (2018).

Similar to their precursors $C_{20}H_{32}N_2O_x$, $C_{30}H_{48}N_4O_x$ showed negligible signal except in period P1, and presented an overlaying time profile of first- and second-generation product pattern (Fig. 6). For comparison, gas-phase trimer products were not observed in the β-pinene $+NO_3$ reaction (Shen et al., 2021), and the trimers observed in SOA from β-pinene $+NO_3$ are likely formed via particle phase reactions (Claflin and Ziemann, 2018). An efficient gas-phase trimer production via subsequent accretion reactions between peroxy radicals requires that the precursor dimer has a high enough reactivity to create a dimer $RO_2^{\bullet}$, e.g., via NO_3 reaction to a double bond. This suggests that the VOC containing at least two double bonds are likely more favorable to form trimers, which is consistent with our previous findings that trimers were formed in the NO_3 reaction with isoprene which also contains two double bonds (Zhao et al., 2021), while they were not observed in the reaction of NO_3 with β-pinene which contains only one double bond (Shen et al., 2021).

3.5 "Primary" incremental HOM yields

We chose period P1 for the calculation of HOM yields in order to minimize the influence of the condensational sink on HOM concentration. However, both first-generation and second-generation products existed in this period, as discussed in Sect. 3.2 through Sect. 3.4 and supported by the time-behavior of the total HOM concentration (Fig. S15). Period P1 can be roughly divided into three phases based on the trends in HOM concentration. Shortly after the limonene injection, large quantities of HOM were produced (first-production phase) followed by a balanced intermediate phase when HOM concentrations stopped increasing. After the intermediate phase, HOM concentrations began to increase again (second-production phase). The first-production phase overlapped with the time span where limonene, NO_3, and N_2O_5 concentrations decreased, implying the dominance of first-generation HOM production process. During the second production period, wall loss was compensated by second-generation HOM formation, leading to another rise of the total HOM concentrations. Therefore, we use the first-production phase to estimate primary HOM production, determined over the first 3 min of the experiment. The calculated "primary" HOM molar yield is $1.5\,\%^{+1.7\,\%}_{-0.7\,\%}$. This value is significantly lower than the HOM yield of 5 % to 17 % in earlier limonene ozonolysis experiments (Ehn et al., 2014; Jokinen et al., 2015; Pagonis et al., 2019). It should be emphasized that second-generation HOM, which contributed greatly to the limonene $+NO_3$ reaction system, is not included in this primary HOM yield.

3.6 Contribution of HOM to particle formation and growth

We observed nucleation and growth of SOA particles in the limonene $+NO_3$ reaction. We calculated the contribution

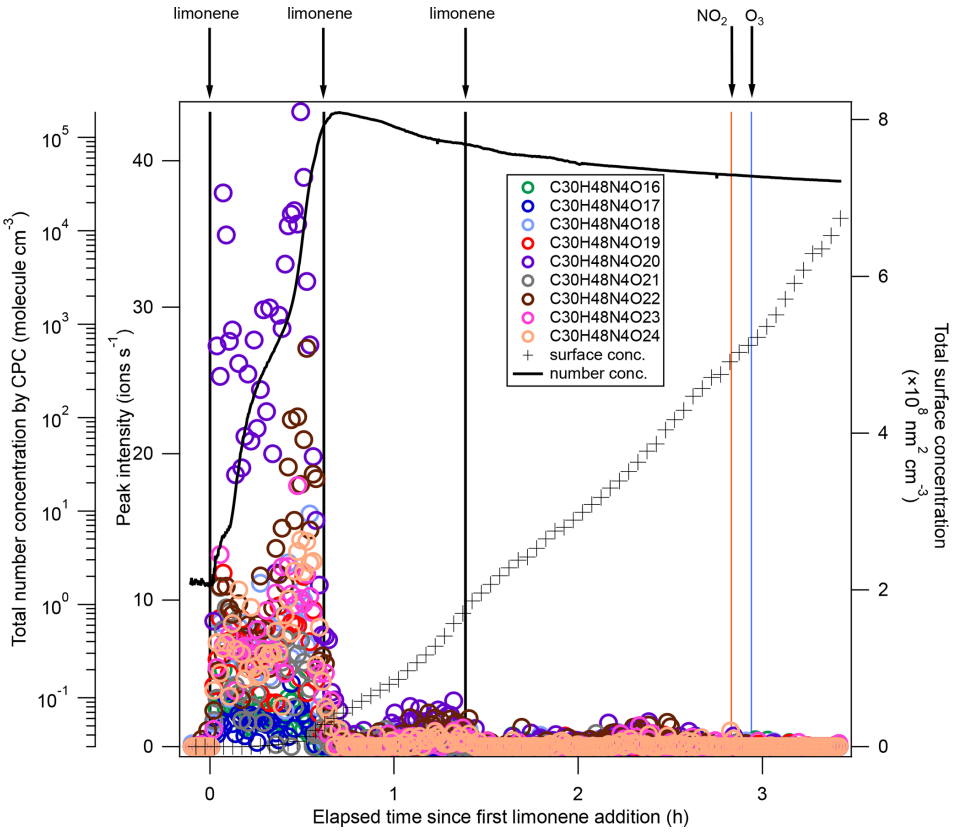

Figure 6. Time series of peak intensity of the $C_{30}H_{48}N_4O_x$ family compounds during the periods P1 to P3. The solid black line refers to total number concentrations detected by CPC. The cross markers (right y axis) indicate total particle surface concentration.

of HOM to SOA formation and particle growth, and compared it to the measured particle growth (Fig. 7a). We assumed different scenarios of HOM uptake on aerosol particles, using the calculation methods described in the literature (Ehn et al., 2014; Seinfeld and Pandis, 2006; Nieminen et al., 2010). The assumption that all HOM irreversibly condense on the particles (scenario 1) resulted in a strong overestimation of particle mass growth (red markers in Fig. 7a). Applying the parameterizations of Mohr et al. (2019) (scenario 2a) or Peräkylä et al. (2020) (scenario 2b) for classification and accounting only LVOC- and ULVOC/ELVOC-HOM for irreversible uptake framed the observed values (blue and yellow markers in Fig. 7a). While scenario 2a agreed quite well with the observations and only slightly overestimated SOA concentrations after 7 h by +11 %, scenario 2b underestimated the SOA concentration at the end by −53 %. The agreement between the modeled and observed SOA concentration suggests that HOM, and particularly LVOC- and ULVOC/ELVOC-HOM, play a major role in growth of SOA particles in this study. This is consistent with the work by Faxon et al. (2018) who found that many of the dimers are ELVOC, which is also supported by our calculation result based on the method of Mohr et al. (2019).

Since neither SO_2 nor H_2SO_4 was added in our experiment, new particle formation (NPF) could be attributed to the nucleation initiated by HOM of low volatility. HOM trimers with as many as 30 carbon atoms were identified in the early stage of this study, and their sudden loss matched the onset of rapid formation of SOA. Trimers identified in our experiment are classified as ULVOC/ELVOC, with much lower volatility than monomers and dimers (Fig. 7b). Therefore, NPF in the current study can more likely be attributed to HOM trimers since they have the strongest potential of initiating nucleation, although we cannot rule out some contributions of dimers in the NPF. In contrast, in an earlier experiment investigating the NO_3-initiated oxidation of β-pinene also conducted in the SAPHIR chamber under similar conditions, new particles were barely formed ($< 20\,cm^{-3}$) (Shen et al., 2021). As already mentioned above, no trimer HOM products were observed in that study, and only molecules with $C \leq 20$ were detected (Sect. 3.4). Extremely low volatile organic vapors formed in α-pinene ozonolysis have been shown to induce nucleation and drive initial particle growth in the atmosphere (Tröstl et al., 2016; Kirkby et al., 2016). Since our experiment of NO_3 oxidation of limonene was performed under near atmospheric conditions, such NPF events induced by the oxidation of limonene by NO_3 could

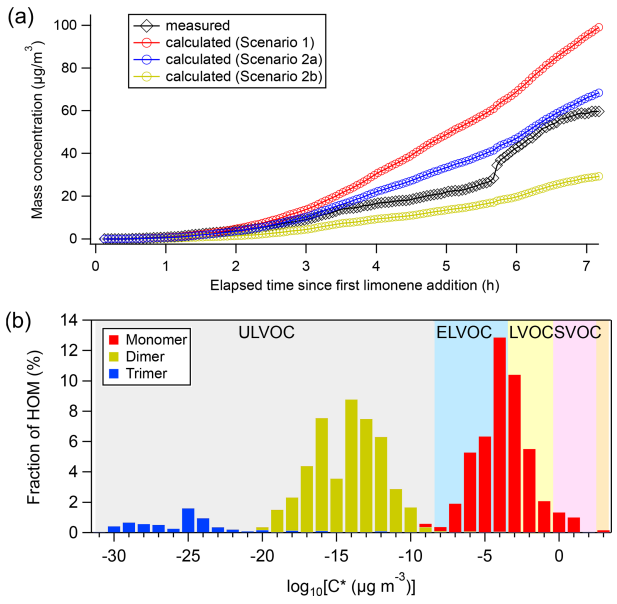

Figure 7. **(a)** Comparison of measured particle concentrations (black) against those predicted from condensation of measured HOM on aerosol particles, where red markers were calculated under scenario 1, and blue and yellow markers were calculated under scenario 2 (only considering the condensation of ULVOC, ELVOC, and LVOC), with the volatility calculated using the method by Mohr et al. (2019) scenario 2a) and Peräkylä et al. (2020) (scenario 2b) respectively. **(b)** HOM volatility distribution using formula provided by Mohr et al. (2019). Average concentrations of HOM in the P1 period were used to calculate the fraction of HOM.

also occur in the ambient atmosphere. Although monoterpene concentrations in this study (0–0.92 ppbv) are higher than in most ambient regions, they are still in the range of ambient concentrations ($\sim$ 0.01–1 ppbv) (e.g., Coggon et al., 2021; Wang et al., 2022), especially for forested regions (e.g., Xu et al., 2015; Kontkanen et al., 2016; Janson, 1992). Assuming that dimers react with NO_3 at a rate similar to limonene, and that they have a condensation sink similar to H_2SO_4 (10^{-3}–10^{-1} s^{-1}) (Dada et al., 2020), the lifetime with respect to NO_3 at an NO_3 concentration of 5–300 ppt and to condensation on particles are $\sim$ 0.1–10 and $\sim$ 0.1–20 min, respectively. Therefore, although aerosols may scavenge HOM dimers in the ambient atmosphere, dimers can still react with NO_3 at nighttime, forming trimers. Such reactions are particularly important when the ambient aerosol concentration is low. Several field observations have shown NPF events taking place at nighttime where biogenic emissions dominate (Kammer et al., 2018; Huang et al., 2019). The work by Ortega et al. (2012) demonstrated an important role of monoterpene ozonolysis products in nocturnal NPF events in chamber experiments. In a previous laboratory study, limonene $+NO_3$ appears more effective at initiating nucleation than the limonene $+O_3$ reaction (Fry et al., 2014), which supports that limonene $+NO_3$ can play a significant role in nighttime nucleation. Our study suggests that NO_3 oxidation of limonene could contribute to the nighttime NPF via HOM trimer formation. In contrast, we infer that NO_3 reactions with other monoterpenes containing only one double bond such as α-pinene and β-pinene are less likely candidates for nighttime NPF, because gas-phase trimers are not observed.

4 Conclusion and implications

HOM formation in the reaction of limonene with NO_3 was investigated in the SAPHIR chamber. About 280 gas-phase HOM products were identified, including monomers (C_{6-10}, O_{6-16}, N_{0-3}), dimers (C_{17-20}, O_{7-20}, N_{0-4}), and trimers (C_{27-30}, O_{16-25}, N_{1-6}). Nitrogen-containing products dominated the HOM, with compounds of the $C_{10}H_{15-17}NO_{6-14}$ series being the most prevalent. Dimers contributed 47 % in the early stage of the experiment when particle surface concentration was rather low ($< 6 \times 10^4$ nm^2 cm^{-3}), which was similar to monomers (47 %). Tentative formation pathways of major families were proposed in this work based on their time-dependent concentration profiles.

In HOM monomers, the abundance of carbonyl compounds significantly exceeded that of hydroxy or hydroperoxy compounds, indicating the significance of unimolecular termination of HOM-RO_2 radicals. Both $RO_2^\bullet$ autoxidation and alkoxy–peroxy pathways were found to be important in the formation of HOM monomers. Monomers with 1 nitrogen atom (1N-monomers) contained both first- and second-generation products, which could be formed via NO_3 oxidation of limonene and its first-generation products, with the latter being more important. Monomers with 2 nitrogen atoms were classified as second-generation products, which could be formed via NO_3 oxidation of the remaining C=C double bond of 1N-monomers.

Dimers showed both first- and second-generation time pattern. Dimers were mostly formed via accretion reactions between monomer RO_2 radicals, resulting in a decrease in O/C ratio compared to monomers. The initial less oxygenated $RO_2^\bullet$, including the $C_{10}H_{16}NO_5^\bullet$ radical that cannot be observed in our instrument, likely played an important role in dimer formation, based on the comparison of measured dimers against expected dimer identity and concentrations according to accretion monomer $RO_2^\bullet$ reactions. Trimers were likely formed via accretion reactions between monomer RO_2 and dimer RO_2 radicals formed from secondary reactions of dimers with NO_3. Trimer formation is thus linked to the presence of two double bonds in limonene, of which the first reacts with NO_3 leading to dimer products while the remaining C=C double bond provides a reactive site for further oxidation of the dimers by NO_3, forming dimer RO_2 radicals.

A "primary" HOM molar yield of $1.5\,\%^{+1.7\,\%}_{-0.7\,\%}$ in the limonene $+NO_3$ reaction was estimated, including only the

first-generation HOM. Second-generation HOM contributed greatly to monomers, dimers, and trimers, and hence the HOM yield we obtained is a lower limit of the total HOM yield, and is likewise much lower than the total HOM yield in the reaction of limonene with ozone (5 % to 17 %) (Ehn et al., 2014; Jokinen et al., 2015; Pagonis et al., 2019).

NPF observed in this work was likely related to the trimer formation due to much lower volatility of trimers compared to monomers and dimers. The SOA concentration in the limonene $+NO_3$ reaction could be explained by the condensation of the HOM belonging to LVOC and ULVOC/ELVOC classes assuming irreversible uptake, indicating an important role of HOM for growth of SOA particles in this reaction system. To our knowledge, this work is the first identifying trimer products from the limonene $+NO_3$ reaction system, suggesting that limonene $+NO_3$ is a possible crucial source of new particles formed in nighttime biogenic emission-dominated areas (Kammer et al., 2018; Huang et al., 2019). Our work highlights the need to consider the role of limonene $+NO_3$ in NPF in models simulating nighttime aerosols formation in biogenic-emission dominated areas, especially with large limonene emissions. In addition, comparison with the reactions of NO_3 with isoprene (Zhao et al., 2021) and other monoterpenes (Shen et al., 2021) reveals a strong dependence of HOM products on the molecular structure of the VOC species in NO_3-initiated chemistry.

The concentration of limonene and NO_3 in this study was on the order of few ppb and a few to 100 ppt, respectively, which are similar to the ambient levels in rural and forest regions affected by anthropogenic emissions (Brown and Stutz, 2012). The chemical lifetime of $RO_2^\bullet$ was of the order of 50 to 500 s, which is also similar to ambient conditions at nighttime (Fry et al., 2018). The $RO_2^\bullet$ loss pathway in our study was dominated by the reactions $RO_2^\bullet + NO_3$ and $RO_2^\bullet + RO_2^\bullet$, which is relevant for the $RO_2^\bullet$ fate in urban areas and forested areas influenced by an urban plume at nighttime. However, in more pristine forested regions, the $RO_2^\bullet$ fate is mostly determined by $RO_2^\bullet + HO_2$ and $RO_2^\bullet + RO_2^\bullet$, as shown by Bates et al. (2022) for the example of a Southeast US forest. As NO_3 concentration is generally enhanced with increased anthropogenic emissions, $RO_2^\bullet + NO_3$ will become more important going from remote to urban areas. Therefore, the HOM products and their formation process in our study are relevant for rural and forested regions influenced by anthropogenic plumes and ambient urban regions with high volatile commercial products emissions, as limonene is a typical component of volatile chemical products (VCPs) (Nazaroff and Weschler, 2004). In these regions, HOM from monoterpene $+NO_3$ reactions can be major components of nighttime SOA. As nitrooxy-RO_2 fate can strongly affect the oxidation product distribution and SOA yield as shown for the reaction of α-pinene with NO_3 (Bates et al., 2022), more studies of HOM formation by NO_3 at various $RO_2^\bullet$ fates are needed to be representative of various environments, including (remote) forested regions.

This study also highlights the important role of second-generation chemistry in HOM formation, which needs to be further investigated and should be included in chemical mechanisms used in numerical models. Additional work is also needed to investigate the role of different HOM formed via NO_3-initiated BVOC oxidation reactions in NPF and growth of SOA particles in order to better constrain the climatic and environmental effects of BVOC $+ NO_3$ chemistry.

Data availability. All the data in the figures and tables of this study are available upon request to the corresponding author (t.mentel@fz-juelich.de or dfzhao@fudan.edu.cn).

Supplement. The supplement related to this article is available online at: https://doi.org/10.5194/acp-22-11323-2022-supplement.

Author contributions. DZ, TFM, and HF designed the study. IP, HF, IHA, RT, FR, and DZ carried out instrument deployment and operation. YG analyzed the MS data and did the MCM simulation with the aid of DZ, HS, and HL. YG, DZ, TFM, and LV interpreted the compiled data set. LV examined the reaction schemes. YG, DZ, TFM, and LV wrote the paper and HS, IP, HL, SK, LV, HF edited the paper. All the co-authors discussed the results and commented on the paper.

Competing interests. The contact author has declared that none of the authors has any competing interests.

Disclaimer. Publisher's note: Copernicus Publications remains neutral with regard to jurisdictional claims in published maps and institutional affiliations.

Acknowledgements. Yindong Guo, Hongru Shen, Hao Luo, and Defeng Zhao would like to thank the funding support of Science and Technology Commission of Shanghai Municipality (no. 20230711400), National Natural Science Foundation of China (no. 41875145), and Shanghai International Science and Technology Partnership Project (no. 21230780200). Sungah Kang, Astrid Kiendler-Scharr, and Thomas F. Mentel acknowledge the support by the EU Project FORCeS (grant agreement no. 821205).

Financial support. This research has been supported by the Science and Technology Commission of Shanghai Municipality (grant nos. 20230711400 and 21230780200), the National Natural Science Foundation of China (grant no. 41875145), and by the EU Project FORCeS (grant agreement no. 821205).

The article processing charges for this open-access publication were covered by the Forschungszentrum Jülich.

Review statement. This paper was edited by Sergey A. Nizkorodov and reviewed by two anonymous referees.

References

Ayres, B. R., Allen, H. M., Draper, D. C., Brown, S. S., Wild, R. J., Jimenez, J. L., Day, D. A., Campuzano-Jost, P., Hu, W., de Gouw, J., Koss, A., Cohen, R. C., Duffey, K. C., Romer, P., Baumann, K., Edgerton, E., Takahama, S., Thornton, J. A., Lee, B. H., Lopez-Hilfiker, F. D., Mohr, C., Wennberg, P. O., Nguyen, T. B., Teng, A., Goldstein, A. H., Olson, K., and Fry, J. L.: Organic nitrate aerosol formation via NO_3+ biogenic volatile organic compounds in the southeastern United States, Atmos. Chem. Phys., 15, 13377–13392, https://doi.org/10.5194/acp-15-13377-2015, 2015.

Bates, K. H., Burke, G. J. P., Cope, J. D., and Nguyen, T. B.: Secondary organic aerosol and organic nitrogen yields from the nitrate radical (NO_3) oxidation of alpha-pinene from various RO_2 fates, Atmos. Chem. Phys., 22, 1467–1482, https://doi.org/10.5194/acp-22-1467-2022, 2022.

Beaver, M. R., Clair, J. M. St., Paulot, F., Spencer, K. M., Crounse, J. D., LaFranchi, B. W., Min, K. E., Pusede, S. E., Wooldridge, P. J., Schade, G. W., Park, C., Cohen, R. C., and Wennberg, P. O.: Importance of biogenic precursors to the budget of organic nitrates: observations of multifunctional organic nitrates by CIMS and TD-LIF during BEARPEX 2009, Atmos. Chem. Phys., 12, 5773–5785, https://doi.org/10.5194/acp-12-5773-2012, 2012.

Bell, D. M., Wu, C., Bertrand, A., Graham, E., Schoonbaert, J., Giannoukos, S., Baltensperger, U., Prevot, A. S. H., Riipinen, I., El Haddad, I., and Mohr, C.: Particle-phase processing of α-pinene NO_3 secondary organic aerosol in the dark, Atmos. Chem. Phys. Discuss. [preprint], https://doi.org/10.5194/acp-2021-379, in review, 2021.

Berkemeier, T., Takeuchi, M., Eris, G., and Ng, N. L.: Kinetic modeling of formation and evaporation of secondary organic aerosol from NO_3 oxidation of pure and mixed monoterpenes, Atmos. Chem. Phys., 20, 15513–15535, https://doi.org/10.5194/acp-20-15513-2020, 2020.

Berndt, T., Mender, B., Scholz, W., Fischer, L., Herrmann, H., Kulmala, M., and Hansel, A.: Accretion Product Formation from Ozonolysis and OH Radical Reaction of α-Pinene: Mechanistic Insight and the Influence of Isoprene and Ethylene, Environ. Sci. Technol., 52, 11069–11077, https://doi.org/10.1021/acs.est.8b02210, 2018a.

Berndt, T., Scholz, W., Mentler, B., Fischer, L., Herrmann, H., Kulmala, M., and Hansel, A.: Accretion Product Formation from Self- and Cross-Reactions of RO_2 Radicals in the Atmosphere, Angew. Chem. Int. Edit., 57, 3820–3824, https://doi.org/10.1002/anie.201710989, 2018b.

Bianchi, F., Kurtén, T., Riva, M., Mohr, C., Rissanen, M. P., Roldin, P., Berndt, T., Crounse, J. D., Wennberg, P. O., Mentel, T. F., Wildt, J., Junninen, H., Jokinen, T., Kulmala, M., Worsnop, D. R., Thornton, J. A., Donahue, N., Kjaergaard, H. G., and Ehn, M.: Highly Oxygenated Organic Molecules (HOM) from Gas-Phase Autoxidation Involving Peroxy Radicals: A Key Contributor to Atmospheric Aerosol, Chem. Rev., 119, 3472–3509, https://doi.org/10.1021/acs.chemrev.8b00395, 2019.

Boyd, C. M., Sanchez, J., Xu, L., Eugene, A. J., Nah, T., Tuet, W. Y., Guzman, M. I., and Ng, N. L.: Secondary organic aerosol formation from the β-pinene+NO_3 system: effect of humidity and peroxy radical fate, Atmos. Chem. Phys., 15, 7497–7522, https://doi.org/10.5194/acp-15-7497-2015, 2015.

Boyd, C. M., Nah, T., Xu, L., Berkemeier, T., and Ng, N. L.: Secondary Organic Aerosol (SOA) from Nitrate Radical Oxidation of Monoterpenes: Effects of Temperature, Dilution, and Humidity on Aerosol Formation, Mixing, and Evaporation, Environ. Sci. Technol., 51, 7831–7841, https://doi.org/10.1021/acs.est.7b01460, 2017.

Brown, S. S. and Stutz, J.: Nighttime radical observations and chemistry, Chem. Soc. Rev., 41, 6405–6447, https://doi.org/10.1039/c2cs35181a, 2012.

Carslaw, N., Mota, T., Jenkin, M. E., Barley, M. H., and McFiggans, G.: A significant role for nitrate and peroxide groups on indoor secondary organic aerosol, Environ. Sci. Technol., 46, 9290–9298, https://doi.org/10.1021/es301350x, 2012.

Chen, Y., Takeuchi, M., Nah, T., Xu, L., Canagaratna, M. R., Stark, H., Baumann, K., Canonaco, F., Prévôt, A. S. H., Huey, L. G., Weber, R. J., and Ng, N. L.: Chemical characterization of secondary organic aerosol at a rural site in the southeastern US: insights from simultaneous high-resolution time-of-flight aerosol mass spectrometer (HR-ToF-AMS) and FIGAERO chemical ionization mass spectrometer (CIMS) measurements, Atmos. Chem. Phys., 20, 8421–8440, https://doi.org/10.5194/acp-20-8421-2020, 2020.

Claflin, M. S. and Ziemann, P. J.: Identification and Quantitation of Aerosol Products of the Reaction of β-Pinene with NO_3 Radicals and Implications for Gas- and Particle-Phase Reaction Mechanisms, J. Phys. Chem. A, 122, 3640–3652, https://doi.org/10.1021/acs.jpca.8b00692, 2018.

Clausen, P. A., Wilkins, C. K., Wolkoff, P., and Nielsen, G. D.: Chemical and biological evaluation of a reaction mixture of $R-(+)$-limonene/ozone: Formation of strong airway irritants, Environ. Int., 26, 511–522, https://doi.org/10.1016/s0160-4120(01)00035-6, 2001.

Coggon, M. M., Gkatzelis, G. I., McDonald, B. C., Gilman, J. B., Schwantes, R. H., Abuhassan, N., Aikin, K. C., Arend, M. F., Berkoff, T. A., Brown, S. S., Campos, T. L., Dickerson, R. R., Gronoff, G., Hurley, J. F., Isaacman-VanWertz, G., Koss, A. R., Li, M., McKeen, S. A., Moshary, F., Peischl, J., Pospisilova, V., Ren, X., Wilson, A., Wu, Y., Trainer, M., and Warneke, C.: Volatile chemical product emissions enhance ozone and modulate urban chemistry, P. Natl. Acad. Sci. USA, 118, e2026653118, https://doi.org/10.1073/pnas.2026653118, 2021.

Crounse, J. D., Nielsen, L. B., Jørgensen, S., Kjaergaard, H. G., and Wennberg, P. O.: Autoxidation of Organic Compounds in the Atmosphere, J. Phys. Chem. Lett., 4, 3513–3520, https://doi.org/10.1021/jz4019207, 2013.

Dada, L., Ylivinkka, I., Baalbaki, R., Li, C., Guo, Y., Yan, C., Yao, L., Sarnela, N., Jokinen, T., Daellenbach, K. R., Yin, R., Deng, C., Chu, B., Nieminen, T., Wang, Y., Lin, Z., Thakur, R. C., Kontkanen, J., Stolzenburg, D., Sipilä, M., Hussein, T., Paasonen, P., Bianchi, F., Salma, I., Weidinger, T., Pikridas, M., Sciare, J., Jiang, J., Liu, Y., Petäjä, T., Kerminen, V.-M., and Kulmala, M.: Sources and sinks driving sulfuric acid concentrations in contrasting environments: implications on proxy calculations, Atmos. Chem. Phys., 20, 11747–11766, https://doi.org/10.5194/acp-20-11747-2020, 2020.

Dam, M., Draper, D. C., Marsavin, A., Fry, J. L., and Smith, J. N.: Observations of gas-phase products from the nitrate-radical-initiated oxidation of four monoterpenes, Atmos. Chem. Phys., 22, 9017–9031, https://doi.org/10.5194/acp-22-9017-2022, 2022.

Donahue, N. M., Epstein, S. A., Pandis, S. N., and Robinson, A. L.: A two-dimensional volatility basis set: 1. organic-aerosol mixing thermodynamics, Atmos. Chem. Phys., 11, 3303–3318, https://doi.org/10.5194/acp-11-3303-2011, 2011.

Donahue, N. M., Kroll, J. H., Pandis, S. N., and Robinson, A. L.: A two-dimensional volatility basis set – Part 2: Diagnostics of organic-aerosol evolution, Atmos. Chem. Phys., 12, 615–634, https://doi.org/10.5194/acp-12-615-2012, 2012.

Ehn, M., Thornton, J. A., Kleist, E., Sipilä, M., Junninen, H., Pullinen, I., Springer, M., Rubach, F., Tillmann, R., Lee, B., Lopez-Hilfiker, F., Andres, S., Acir, I. H., Rissanen, M., Jokinen, T., Schobesberger, S., Kangasluoma, J., Kontkanen, J., Nieminen, T., Kurtén, T., Nielsen, L. B., Jørgensen, S., Kjaergaard, H. G., Canagaratna, M., Dal Maso, M., Berndt, T., Petäjä, T., Wahner, A., Kerminen, V. M., Kulmala, M., Worsnop, D. R., Wildt, J., and Mentel, T. F.: A large source of low-volatility secondary organic aerosol, Nature, 506, 476–485, https://doi.org/10.1038/nature13032, 2014.

Eisele, F. L. and Tanner, D. J.: Measurement of the gas phase concentration of H_2SO_4 and methane sulfonic acid and estimates of H_2SO_4 production and loss in the atmosphere, J. Geophys. Res.-Atmos., 98, 9001–9010, https://doi.org/10.1029/93jd00031, 1993.

Fan, Z. H., Lioy, P., Weschler, C., Fiedler, N., Kipen, H., and Zhang, J. F.: Ozone-initiated reactions with mixtures of volatile organic compounds under simulated indoor conditions, Environ. Sci. Technol., 37, 1811–1821, https://doi.org/10.1021/es026231i, 2003.

Faxon, C., Hammes, J., Le Breton, M., Pathak, R. K., and Hallquist, M.: Characterization of organic nitrate constituents of secondary organic aerosol (SOA) from nitrate-radical-initiated oxidation of limonene using high-resolution chemical ionization mass spectrometry, Atmos. Chem. Phys., 18, 5467–5481, https://doi.org/10.5194/acp-18-5467-2018, 2018.

Finlayson-Pitts, B. J. and Pitts, J. N.: Tropospheric air pollution: Ozone, airborne toxics, polycyclic aromatic hydrocarbons, and particles, Science, 276, 1045–1052, https://doi.org/10.1126/science.276.5315.1045, 1997.

Fry, J. L., Kiendler-Scharr, A., Rollins, A. W., Wooldridge, P. J., Brown, S. S., Fuchs, H., Dubé, W., Mensah, A., dal Maso, M., Tillmann, R., Dorn, H.-P., Brauers, T., and Cohen, R. C.: Organic nitrate and secondary organic aerosol yield from NO_3 oxidation of β-pinene evaluated using a gas-phase kinetics/aerosol partitioning model, Atmos. Chem. Phys., 9, 1431–1449, https://doi.org/10.5194/acp-9-1431-2009, 2009.

Fry, J. L., Kiendler-Scharr, A., Rollins, A. W., Brauers, T., Brown, S. S., Dorn, H.-P., Dubé, W. P., Fuchs, H., Mensah, A., Rohrer, F., Tillmann, R., Wahner, A., Wooldridge, P. J., and Cohen, R. C.: SOA from limonene: role of NO_3 in its generation and degradation, Atmos. Chem. Phys., 11, 3879–3894, https://doi.org/10.5194/acp-11-3879-2011, 2011.

Fry, J. L., Draper, D. C., Zarzana, K. J., Campuzano-Jost, P., Day, D. A., Jimenez, J. L., Brown, S. S., Cohen, R. C., Kaser, L., Hansel, A., Cappellin, L., Karl, T., Hodzic Roux, A., Turnipseed, A., Cantrell, C., Lefer, B. L., and Grossberg, N.: Observations of gas- and aerosol-phase organic nitrates at BEACHON-RoMBAS 2011, Atmos. Chem. Phys., 13, 8585–8605, https://doi.org/10.5194/acp-13-8585-2013, 2013.

Fry, J. L., Draper, D. C., Barsanti, K. C., Smith, J. N., Ortega, J., Winkler, P. M., Lawler, M. J., Brown, S. S., Edwards, P. M., Cohen, R. C., and Lee, L.: Secondary organic aerosol formation and organic nitrate yield from NO_3 oxidation of biogenic hydrocarbons, Environ. Sci. Technol., 48, 11944–11953, https://doi.org/10.1021/es502204x, 2014.

Fry, J. L., Brown, S. S., Middlebrook, A. M., Edwards, P. M., Campuzano-Jost, P., Day, D. A., Jimenez, J. L., Allen, H. M., Ryerson, T. B., Pollack, I., Graus, M., Warneke, C., de Gouw, J. A., Brock, C. A., Gilman, J., Lerner, B. M., Dubé, W. P., Liao, J., and Welti, A.: Secondary organic aerosol (SOA) yields from NO_3 radical + isoprene based on nighttime aircraft power plant plume transects, Atmos. Chem. Phys., 18, 11663–11682, https://doi.org/10.5194/acp-18-11663-2018, 2018.

Fuchs, H., Hofzumahaus, A., Rohrer, F., Bohn, B., Brauers, T., Dorn, H. P., Häseler, R., Holland, F., Kaminski, M., Li, X., Lu, K., Nehr, S., Tillmann, R., Wegener, R., and Wahner, A.: Experimental evidence for efficient hydroxyl radical regeneration in isoprene oxidation, Nat. Geosci., 6, 1023–1026, https://doi.org/10.1038/ngeo1964, 2013.

Fuchs, N. A., and Sutugin, A. G.: High dispersed aerosols, in: Topics in Current Aerosol Research, edited by: Hidy, G. M. and Brock, J. R., Pergamon, New York, ISBN: 1483146170, 1971.

Gkatzelis, G. I., Coggon, M. M., McDonald, B. C., Peischl, J., Aikin, K. C., Gilman, J. B., Trainer, M., and Warneke, C.: Identifying Volatile Chemical Product Tracer Compounds in U.S. Cities, Environ. Sci. Technol., 55, 188–199, https://doi.org/10.1021/acs.est.0c05467, 2021.

Guenther, A. B., Jiang, X., Heald, C. L., Sakulyanontvittaya, T., Duhl, T., Emmons, L. K., and Wang, X.: The Model of Emissions of Gases and Aerosols from Nature version 2.1 (MEGAN2.1): an extended and updated framework for modeling biogenic emissions, Geosci. Model Dev., 5, 1471–1492, https://doi.org/10.5194/gmd-5-1471-2012, 2012.

Hallquist, M., Wängberg, I., Ljungström, E., Barnes, I., and Becker, K. H.: Aerosol and product yields from NO_3 radical-initiated oxidation of selected monoterpenes, Environ. Sci. Technol., 33, 553–559, https://doi.org/10.1021/es980292s, 1999.

Hallquist, M., Wenger, J. C., Baltensperger, U., Rudich, Y., Simpson, D., Claeys, M., Dommen, J., Donahue, N. M., George, C., Goldstein, A. H., Hamilton, J. F., Herrmann, H., Hoffmann, T., Iinuma, Y., Jang, M., Jenkin, M. E., Jimenez, J. L., Kiendler-Scharr, A., Maenhaut, W., McFiggans, G., Mentel, Th. F., Monod, A., Prévôt, A. S. H., Seinfeld, J. H., Surratt, J. D., Szmigielski, R., and Wildt, J.: The formation, properties and impact of secondary organic aerosol: current and emerging issues, Atmos. Chem. Phys., 9, 5155–5236, https://doi.org/10.5194/acp-9-5155-2009, 2009.

Huang, W., Saathoff, H., Shen, X., Ramisetty, R., Leisner, T., and Mohr, C.: Chemical Characterization of Highly Functionalized Organonitrates Contributing to Night-Time Organic Aerosol Mass Loadings and Particle Growth, Environ. Sci. Technol., 53, 1165–1174, https://doi.org/10.1021/acs.est.8b05826, 2019.

Hyttinen, N., Kupiainen-Määttä, O., Rissanen, M. P., Muuronen, M., Ehn, M., and Kurtén, T.: Modeling the Charging

of Highly Oxidized Cyclohexene Ozonolysis Products Using Nitrate-Based Chemical Ionization, J. Phys. Chem. A, 119, 6339–6345, https://doi.org/10.1021/acs.jpca.5b01818, 2015.

Janson, R.: Monoterpene concentrations in and above a forest of scots pine, J. Atmos. Chem., 14, 385–394, https://doi.org/10.1007/bf00115246, 1992.

Jenkin, M. E., Saunders, S. M., and Pilling, M. J.: The tropospheric degradation of volatile organic compounds: A protocol for mechanism development, Atmos. Environ., 31, 81–104, https://doi.org/10.1016/s1352-2310(96)00105-7, 1997.

Jiang, L., Wang, W., and Xu, Y. S.: Theoretical investigation of the NO_3 radical addition to double bonds of limonene, Int. J. Mol. Sci., 10, 3743–3754, https://doi.org/10.3390/ijms10093743, 2009.

Jokinen, T., Sipilä, M., Junninen, H., Ehn, M., Lönn, G., Hakala, J., Petäjä, T., Mauldin III, R. L., Kulmala, M., and Worsnop, D. R.: Atmospheric sulphuric acid and neutral cluster measurements using CI-APi-TOF, Atmos. Chem. Phys., 12, 4117–4125, https://doi.org/10.5194/acp-12-4117-2012, 2012.

Jokinen, T., Berndt, T., Makkonen, R., Kerminen, V. M., Junninen, H., Paasonen, P., Stratmann, F., Herrmann, H., Guenther, A. B., Worsnop, D. R., Kulmala, M., Ehn, M., and Sipilä, M.: Production of extremely low volatile organic compounds from biogenic emissions: Measured yields and atmospheric implications, P. Natl. Acad. Sci. USA, 112, 7123–7128, https://doi.org/10.1073/pnas.1423977112, 2015.

Kammer, J., Perraudin, E., Flaud, P. M., Lamaud, E., Bonnefond, J. M., and Villenave, E.: Observation of nighttime new particle formation over the French Landes forest, Sci. Total Environ., 621, 1084–1092, https://doi.org/10.1016/j.scitotenv.2017.10.118, 2018.

Kirkby, J., Duplissy, J., Sengupta, K., Frege, C., Gordon, H., Williamson, C., Heinritzi, M., Simon, M., Yan, C., Almeida, J., Tröstl, J., Nieminen, T., Ortega, I. K., Wagner, R., Adamov, A., Amorim, A., Bernhammer, A. K., Bianchi, F., Breitenlechner, M., Brilke, S., Chen, X., Craven, J., Dias, A., Ehrhart, S., Flagan, R. C., Franchin, A., Fuchs, C., Guida, R., Hakala, J., Hoyle, C. R., Jokinen, T., Junninen, H., Kangasluoma, J., Kim, J., Krapf, M., Kürten, A., Laaksonen, A., Lehtipalo, K., Makhmutov, V., Mathot, S., Molteni, U., Onnela, A., Peräkylä, O., Piel, F., Petäjä, T., Praplan, A. P., Pringle, K., Rap, A., Richards, N. A., Riipinen, I., Rissanen, M. P., Rondo, L., Sarnela, N., Schobesberger, S., Scott, C. E., Seinfeld, J. H., Sipilä, M., Steiner, G., Stozhkov, Y., Stratmann, F., Tomé, A., Virtanen, A., Vogel, A. L., Wagner, A. C., Wagner, P. E., Weingartner, E., Wimmer, D., Winkler, P. M., Ye, P., Zhang, X., Hansel, A., Dommen, J., Donahue, N. M., Worsnop, D. R., Baltensperger, U., Kulmala, M., Carslaw, K. S., and Curtius, J.: Ion-induced nucleation of pure biogenic particles, Nature, 533, 521–526, https://doi.org/10.1038/nature17953, 2016.

Klinger, L. F., Li, Q. J., Guenther, A. B., Greenberg, J. P., Baker, B., and Bai, J. H.: Assessment of volatile organic compound emissions from ecosystems of China, J. Geophys. Res.-Atmos., 107, 4603, https://doi.org/10.1029/2001jd001076, 2002.

Kontkanen, J., Paasonen, P., Aalto, J., Bäck, J., Rantala, P., Petäjä, T., and Kulmala, M.: Simple proxies for estimating the concentrations of monoterpenes and their oxidation products at a boreal forest site, Atmos. Chem. Phys., 16, 13291–13307, https://doi.org/10.5194/acp-16-13291-2016, 2016.

Kulmala, M., Petäjä, T., Nieminen, T., Sipilä, M., Manninen, H. E., Lehtipalo, K., Dal Maso, M., Aalto, P. P., Junninen, H., Paasonen, P., Riipinen, I., Lehtinen, K. E. J., Laaksonen, A., and Kerminen, V.-M.: Measurement of the nucleation of atmospheric aerosol particles, Nat. Protoc., 7, 1651–1667, https://doi.org/10.1038/nprot.2012.091, 2012.

Kurtén, T., Møller, K. H., Nguyen, T. B., Schwantes, R. H., Misztal, P. K., Su, L., Wennberg, P. O., Fry, J. L., and Kjaergaard, H. G.: Alkoxy Radical Bond Scissions Explain the Anomalously Low Secondary Organic Aerosol and Organonitrate Yields From α-Pinene + NO_3, J. Phys. Chem. Lett., 8, 2826–2834, https://doi.org/10.1021/acs.jpclett.7b01038, 2017.

Lee, B. H., Mohr, C., Lopez-Hilfiker, F. D., Lutz, A., Hallquist, M., Lee, L., Romer, P., Cohen, R. C., Iyer, S., Kurten, T., Hu, W., Day, D. A., Campuzano-Jost, P., Jimenez, J. L., Xu, L., Ng, N. L., Guo, H., Weber, R. J., Wild, R. J., Brown, S. S., Koss, A., de Gouw, J., Olson, K., Goldstein, A. H., Seco, R., Kim, S., McAvey, K., Shepson, P. B., Starn, T., Baumann, K., Edgerton, E. S., Liu, J., Shilling, J. E., Miller, D. O., Brune, W., Schobesberger, S., D'Ambro, E. L., and Thornton, J. A.: Highly functionalized organic nitrates in the southeast United States: Contribution to secondary organic aerosol and reactive nitrogen budgets, P. Natl. Acad. Sci. USA, 113, 1516–1521, https://doi.org/10.1073/pnas.1508108113, 2016.

Liu, Y., Nie, W., Li, Y., Ge, D., Liu, C., Xu, Z., Chen, L., Wang, T., Wang, L., Sun, P., Qi, X., Wang, J., Xu, Z., Yuan, J., Yan, C., Zhang, Y., Huang, D., Wang, Z., Donahue, N. M., Worsnop, D., Chi, X., Ehn, M., and Ding, A.: Formation of condensable organic vapors from anthropogenic and biogenic volatile organic compounds (VOCs) is strongly perturbed by NO_x in eastern China, Atmos. Chem. Phys., 21, 14789–14814, https://doi.org/10.5194/acp-21-14789-20211, 2021.

Massoli, P., Stark, H., Canagaratna, M. R., Krechmer, J. E., Xu, L., Ng, N. L., Mauldin, R. L., Yan, C., Kimmel, J., Misztal, P. K., Jimenez, J. L., Jayne, J. T., and Worsnop, D. R.: Ambient Measurements of Highly Oxidized Gas-Phase Molecules during the Southern Oxidant and Aerosol Study (SOAS) 2013, ACS Earth Space Chem., 2, 653–672, https://doi.org/10.1021/acsearthspacechem.8b00028, 2018.

McDonald, B. C., de Gouw, J. A., Gilman, J. B., Jathar, S. H., Akherati, A., Cappa, C. D., Jimenez, J. L., Lee-Taylor, J., Hayes, P. L., McKeen, S. A., Cui, Y. Y., Kim, S.-W., Gentner, D. R., Isaacman-VanWertz, G., Goldstein, A. H., Harley, R. A., Frost, G. J., Roberts, J. M., Ryerson, T. B., and Trainer, M.: Volatile chemical products emerging as largest petrochemical source of urban organic emissions, Science, 359, 760–764, https://doi.org/10.1126/science.aaq0524, 2018.

McFiggans, G., Mentel, T. F., Wildt, J., Pullinen, I., Kang, S., Kleist, E., Schmitt, S., Springer, M., Tillmann, R., Wu, C., Zhao, D. F., Hallquist, M., Faxon, C., Le Breton, M., Hallquist, A. M., Simpson, D., Bergström, R., Jenkin, M. E., Ehn, M., Thornton, J. A., Alfarra, M. R., Bannan, T. J., Percival, C. J., Priestley, M., Topping, D., and Kiendler-Scharr, A.: Secondary organic aerosol reduced by mixture of atmospheric vapours, Nature, 565, 587–593, https://doi.org/10.1038/s41586-018-0871-y, 2019.

Mentel, T. F., Springer, M., Ehn, M., Kleist, E., Pullinen, I., Kurtén, T., Rissanen, M., Wahner, A., and Wildt, J.: Formation of highly oxidized multifunctional compounds: autoxidation of peroxy radicals formed in the ozonolysis of alkenes – deduced from

structure–product relationships, Atmos. Chem. Phys., 15, 6745–6765, https://doi.org/10.5194/acp-15-6745-2015, 2015.

Mohr, C., Thornton, J. A., Heitto, A., Lopez-Hilfiker, F. D., Lutz, A., Riipinen, I., Hong, J., Donahue, N. M., Hallquist, M., Petäjä, T., Kulmala, M., and Yli-Juuti, T.: Molecular identification of organic vapors driving atmospheric nanoparticle growth, Nat. Commun., 10, 4442, https://doi.org/10.1038/s41467-019-12473-2, 2019.

Mutzel, A., Zhang, Y., Böge, O., Rodigast, M., Kolodziejczyk, A., Wang, X., and Herrmann, H.: Importance of secondary organic aerosol formation of α-pinene, limonene, and *m*-cresol comparing day- and nighttime radical chemistry, Atmos. Chem. Phys., 21, 8479–8498, https://doi.org/10.5194/acp-21-8479-2021, 2021.

Nah, T., Sanchez, J., Boyd, C. M., and Ng, N. L.: Photochemical Aging of α-pinene and β-pinene Secondary Organic Aerosol formed from Nitrate Radical Oxidation, Environ. Sci. Technol., 50, 222–231, https://doi.org/10.1021/acs.est.5b04594, 2016.

Nazaroff, W. W. and Weschler, C. J.: Cleaning products and air fresheners: exposure to primary and secondary air pollutants, Atmos. Environ., 38, 2841–2865, https://doi.org/10.1016/j.atmosenv.2004.02.040, 2004.

Ng, N. L., Kwan, A. J., Surratt, J. D., Chan, A. W. H., Chhabra, P. S., Sorooshian, A., Pye, H. O. T., Crounse, J. D., Wennberg, P. O., Flagan, R. C., and Seinfeld, J. H.: Secondary organic aerosol (SOA) formation from reaction of isoprene with nitrate radicals (NO_3), Atmos. Chem. Phys., 8, 4117–4140, https://doi.org/10.5194/acp-8-4117-2008, 2008.

Nie, W., Yan, C., Huang, D. D., Wang, Z., Liu, Y., Qiao, X., Guo, Y., Tian, L., Zheng, P., Xu, Z., Li, Y., Xu, Z., Qi, X., Sun, P., Wang, J., Zheng, F., Li, X., Yin, R., Dallenbach, K. R., Bianchi, F., Petäjä, T., Zhang, Y., Wang, M., Schervish, M., Wang, S., Qiao, L., Wang, Q., Zhou, M., Wang, H., Yu, C., Yao, D., Guo, H., Ye, P., Lee, S., Li, Y. J., Liu, Y., Chi, X., Kerminen, V.-M., Ehn, M., Donahue, N. M., Wang, T., Huang, C., Kulmala, M., Worsnop, D., Jiang, J., and Ding, A.: Secondary organic aerosol formed by condensing anthropogenic vapours over China's megacities, Nat. Geosci., 15, 255–261, https://doi.org/10.1038/s41561-022-00922-5, 2022.

Nieminen, T., Lehtinen, K. E. J., and Kulmala, M.: Sub-10 nm particle growth by vapor condensation – effects of vapor molecule size and particle thermal speed, Atmos. Chem. Phys., 10, 9773–9779, https://doi.org/10.5194/acp-10-9773-2010, 2010.

Novelli, A., Cho, C., Fuchs, H., Hofzumahaus, A., Rohrer, F., Tillmann, R., Kiendler-Scharr, A., Wahner, A., and Vereecken, L.: Experimental and theoretical study on the impact of a nitrate group on the chemistry of alkoxy radicals, Phys. Chem. Chem. Phys., 23, 5474–5495, https://doi.org/10.1039/d0cp05555g, 2021.

Ortega, I. K., Suni, T., Boy, M., Grönholm, T., Manninen, H. E., Nieminen, T., Ehn, M., Junninen, H., Hakola, H., Hellén, H., Valmari, T., Arvela, H., Zegelin, S., Hughes, D., Kitchen, M., Cleugh, H., Worsnop, D. R., Kulmala, M., and Kerminen, V.-M.: New insights into nocturnal nucleation, Atmos. Chem. Phys., 12, 4297–4312, https://doi.org/10.5194/acp-12-4297-2012, 2012.

Pagonis, D., Algrim, L. B., Price, D. J., Day, D. A., Handschy, A. V., Stark, H., Miller, S. L., de Gouw, J. A., Jimenez, J. L., and Ziemann, P. J.: Autoxidation of Limonene Emitted in a University Art Museum, Environ. Sci. Tech. Let., 6, 520–524, https://doi.org/10.1021/acs.estlett.9b00425, 2019.

Peng, C., Wang, W., Li, K., Li, J., Zhou, L., Wang, L., and Ge, M.: The Optical Properties of Limonene Secondary Organic Aerosols: The Role of NO_3, OH, and O_3 in the Oxidation Processes, J. Geophys. Res.-Atmos., 123, 3292–3303, https://doi.org/10.1002/2017JD028090, 2018.

Peräkylä, O., Riva, M., Heikkinen, L., Quéléver, L., Roldin, P., and Ehn, M.: Experimental investigation into the volatilities of highly oxygenated organic molecules (HOMs), Atmos. Chem. Phys., 20, 649–669, https://doi.org/10.5194/acp-20-649-2020, 2020.

Pullinen, I., Schmitt, S., Kang, S., Sarrafzadeh, M., Schlag, P., Andres, S., Kleist, E., Mentel, T. F., Rohrer, F., Springer, M., Tillmann, R., Wildt, J., Wu, C., Zhao, D., Wahner, A., and Kiendler-Scharr, A.: Impact of NO_x on secondary organic aerosol (SOA) formation from α-pinene and β-pinene photooxidation: the role of highly oxygenated organic nitrates, Atmos. Chem. Phys., 20, 10125–10147, https://doi.org/10.5194/acp-20-10125-2020, 2020.

Pye, H. O. T., Chan, A. W. H., Barkley, M. P., and Seinfeld, J. H.: Global modeling of organic aerosol: the importance of reactive nitrogen (NO_x and NO_3), Atmos. Chem. Phys., 10, 11261–11276, https://doi.org/10.5194/acp-10-11261-2010, 2010.

Rissanen, M. P., Kurtén, T., Sipilä, M., Thornton, J. A., Kangasluoma, J., Sarnela, N., Junninen, H., Jørgensen, S., Schallhart, S., Kajos, M. K., Taipale, R., Springer, M., Mentel, T. F., Ruuskanen, T., Petäjä, T., Worsnop, D. R., Kjaergaard, H. G., and Ehn, M.: The formation of highly oxidized multifunctional products in the ozonolysis of cyclohexene, J. Am. Chem. Soc., 136, 15596–15606, https://doi.org/10.1021/ja507146s, 2014.

Riva, M., Rantala, P., Krechmer, J. E., Peräkylä, O., Zhang, Y., Heikkinen, L., Garmash, O., Yan, C., Kulmala, M., Worsnop, D., and Ehn, M.: Evaluating the performance of five different chemical ionization techniques for detecting gaseous oxygenated organic species, Atmos. Meas. Tech., 12, 2403–2421, https://doi.org/10.5194/amt-12-2403-2019, 2019.

Rohrer, F., Bohn, B., Brauers, T., Brüning, D., Johnen, F.-J., Wahner, A., and Kleffmann, J.: Characterisation of the photolytic HONO-source in the atmosphere simulation chamber SAPHIR, Atmos. Chem. Phys., 5, 2189–2201, https://doi.org/10.5194/acp-5-2189-2005, 2005.

Rollins, A. W., Kiendler-Scharr, A., Fry, J. L., Brauers, T., Brown, S. S., Dorn, H.-P., Dubé, W. P., Fuchs, H., Mensah, A., Mentel, T. F., Rohrer, F., Tillmann, R., Wegener, R., Wooldridge, P. J., and Cohen, R. C.: Isoprene oxidation by nitrate radical: alkyl nitrate and secondary organic aerosol yields, Atmos. Chem. Phys., 9, 6685–6703, https://doi.org/10.5194/acp-9-6685-2009, 2009.

Rollins, A. W., Browne, E. C., Min, K.-E., Pusede, S. E., Wooldridge, P. J., Gentner, D. R., Goldstein, A. H., Liu, S., Day, D. A., Russell, L. M., and Cohen, R. C.: Evidence for NO_x control over nighttime SOA formation, Science, 337, 1210–1212, https://doi.org/10.1126/science.1221520, 2012.

Saunders, S. M., Jenkin, M. E., Derwent, R. G., and Pilling, M. J.: Protocol for the development of the Master Chemical Mechanism, MCM v3 (Part A): tropospheric degradation of non-aromatic volatile organic compounds, Atmos. Chem. Phys., 3, 161-180, 2003.

Schervish, M. and Donahue, N. M.: Peroxy radical chemistry and the volatility basis set, Atmos. Chem. Phys., 20, 1183–1199, https://doi.org/10.5194/acp-20-1183-2020, 2020.

Seinfeld, J. H. and Pandis, S. N.: Atmospheric Chemistry and Physics: From Air Pollution to Climate Change, 2nd edn., Wiley, John & Sons, New York, ISBN: 0-471-72018-6, 2006.

Shen, H., Zhao, D., Pullinen, I., Kang, S., Vereecken, L., Fuchs, H., Acir, I.-H., Tillmann, R., Rohrer, F., Wildt, J., Kiendler-Scharr, A., Wahner, A., and Mentel, T. F.: Highly Oxygenated Organic Nitrates Formed from NO_3 Radical-Initiated Oxidation of β-Pinene, Environ. Sci. Technol., 55, 15658–15671, https://doi.org/10.1021/acs.est.1c03978, 2021.

Shrivastava, M., Cappa, C. D., Fan, J., Goldstein, A. H., Guenther, A. B., Jimenez, J. L., Kuang, C., Laskin, A., Martin, S. T., Ng, N. L., Petäjä, T., Pierce, J. R., Rasch, P. J., Roldin, P., Seinfeld, J. H., Shilling, J., Smith, J. N., Thornton, J. A., Volkamer, R., Wang, J., Worsnop, D. R., Zaveri, R. A., Zelenyuk, A., and Zhang, Q.: Recent advances in understanding secondary organic aerosol: Implications for global climate forcing, Rev. Geophys., 55, 509–559, https://doi.org/10.1002/2016rg000540, 2017.

Slade, J. H., de Perre, C., Lee, L., and Shepson, P. B.: Nitrate radical oxidation of γ-terpinene: hydroxy nitrate, total organic nitrate, and secondary organic aerosol yields, Atmos. Chem. Phys., 17, 8635–8650, https://doi.org/10.5194/acp-17-8635-2017, 2017.

Spittler, M., Barnes, I., Bejan, I., Brockmann, K. J., Benter, T., and Wirtz, K.: Reactions of NO_3 radicals with limonene and α-pinene: Product and SOA formation, Atmos. Environ., 40, 116–127, https://doi.org/10.1016/j.atmosenv.2005.09.093, 2006.

Takeuchi, M. and Ng, N. L.: Chemical composition and hydrolysis of organic nitrate aerosol formed from hydroxyl and nitrate radical oxidation of α-pinene and β-pinene, Atmos. Chem. Phys., 19, 12749–12766, https://doi.org/10.5194/acp-19-12749-2019, 2019.

Tröstl, J., Chuang, W. K., Gordon, H., Heinritzi, M., Yan, C., Molteni, U., Ahlm, L., Frege, C., Bianchi, F., Wagner, R., Simon, M., Lehtipalo, K., Williamson, C., Craven, J. S., Duplissy, J., Adamov, A., Almeida, J., Bernhammer, A. K., Breitenlechner, M., Brilke, S., Dias, A., Ehrhart, S., Flagan, R. C., Franchin, A., Fuchs, C., Guida, R., Gysel, M., Hansel, A., Hoyle, C. R., Jokinen, T., Junninen, H., Kangasluoma, J., Keskinen, H., Kim, J., Krapf, M., Kürten, A., Laaksonen, A., Lawler, M., Leiminger, M., Mathot, S., Möhler, O., Nieminen, T., Onnela, A., Petäjä, T., Piel, F. M., Miettinen, P., Rissanen, M. P., Rondo, L., Sarnela, N., Schobesberger, S., Sengupta, K., Sipilä, M., Smith, J. N., Steiner, G., Tomè, A., Virtanen, A., Wagner, A. C., Weingartner, E., Wimmer, D., Winkler, P. M., Ye, P., Carslaw, K. S., Curtius, J., Dommen, J., Kirkby, J., Kulmala, M., Riipinen, I., Worsnop, D. R., Donahue, N. M., and Baltensperger, U.: The role of low-volatility organic compounds in initial particle growth in the atmosphere, Nature, 533, 527–531, https://doi.org/10.1038/nature18271, 2016.

Vereecken, L. and Nozière, B.: H migration in peroxy radicals under atmospheric conditions, Atmos. Chem. Phys., 20, 7429–7458, https://doi.org/10.5194/acp-20-7429-2020, 2020.

Vereecken, L. and Peeters, J.: Decomposition of substituted alkoxy radicals-part I: a generalized structure-activity relationship for reaction barrier heights, Phys. Chem. Chem. Phys., 11, 9062–9074, https://doi.org/10.1039/b909712k, 2009.

Vereecken, L. and Peeters, J.: A structure-activity relationship for the rate coefficient of H-migration in substituted alkoxy radicals, Phys. Chem. Chem. Phys., 12, 12608–12620, https://doi.org/10.1039/c0cp00387e, 2010.

Wagner, N. L., Dubé, W. P., Washenfelder, R. A., Young, C. J., Pollack, I. B., Ryerson, T. B., and Brown, S. S.: Diode laser-based cavity ring-down instrument for NO_3, N_2O_5, NO, NO_2 and O_3 from aircraft, Atmos. Meas. Tech., 4, 1227–1240, https://doi.org/10.5194/amt-4-1227-2011, 2011.

Wang, H., Ma, X., Tan, Z., Wang, H., Chen, X., Chen, S., Gao, Y., Liu, Y., Liu, Y., Yang, X., Yuan, B., Zeng, L., Huang, C., Lu, K., and Zhang, Y.: Anthropogenic monoterpenes aggravating ozone pollution, Natl. Sci. Rev., nwac103, https://doi.org/10.1093/nsr/nwac103, 2022.

Wang, S. and Pratt, K. A.: Molecular Halogens Above the Arctic Snowpack: Emissions, Diurnal Variations, and Recycling Mechanisms, J. Geophys. Res.-Atmos., 122, 11991–12007, https://doi.org/10.1002/2017jd027175, 2017.

Wu, C., Bell, D. M., Graham, E. L., Haslett, S., Riipinen, I., Baltensperger, U., Bertrand, A., Giannoukos, S., Schoonbaert, J., El Haddad, I., Prevot, A. S. H., Huang, W., and Mohr, C.: Photolytically induced changes in composition and volatility of biogenic secondary organic aerosol from nitrate radical oxidation during night-to-day transition, Atmos. Chem. Phys., 21, 14907–14925, https://doi.org/10.5194/acp-21-14907-2021, 2021.

Wu, R., Vereecken, L., Tsiligiannis, E., Kang, S., Albrecht, S. R., Hantschke, L., Zhao, D., Novelli, A., Fuchs, H., Tillmann, R., Hohaus, T., Carlsson, P. T. M., Shenolikar, J., Bernard, F., Crowley, J. N., Fry, J. L., Brownwood, B., Thornton, J. A., Brown, S. S., Kiendler-Scharr, A., Wahner, A., Hallquist, M., and Mentel, T. F.: Molecular composition and volatility of multi-generation products formed from isoprene oxidation by nitrate radical, Atmos. Chem. Phys., 21, 10799–10824, https://doi.org/10.5194/acp-21-10799-2021, 2021.

Xu, L., Guo, H., Boyd, C. M., Klein, M., Bougiatioti, A., Cerully, K. M., Hite, J. R., Isaacman-VanWertz, G., Kreisberg, N. M., Knote, C., Olson, K., Koss, A., Goldstein, A. H., Hering, S. V., de Gouw, J., Baumann, K., Lee, S.-H., Nenes, A., Weber, R. J., and Ng, N. L.: Effects of anthropogenic emissions on aerosol formation from isoprene and monoterpenes in the southeastern United States, P. Natl. Acad. Sci. USA, 112, 37–42, https://doi.org/10.1073/pnas.1417609112, 2015.

Yan, C., Nie, W., Äijälä, M., Rissanen, M. P., Canagaratna, M. R., Massoli, P., Junninen, H., Jokinen, T., Sarnela, N., Häme, S. A. K., Schobesberger, S., Canonaco, F., Yao, L., Prévôt, A. S. H., Petäjä, T., Kulmala, M., Sipilä, M., Worsnop, D. R., and Ehn, M.: Source characterization of highly oxidized multifunctional compounds in a boreal forest environment using positive matrix factorization, Atmos. Chem. Phys., 16, 12715–12731, https://doi.org/10.5194/acp-16-12715-2016, 2016.

Zhang, H., Yee, L. D., Lee, B. H., Curtis, M. P., Worton, D. R., Isaacman-VanWertz, G., Offenberg, J. H., Lewandowski, M., Kleindienst, T. E., Beaver, M. R., Holder, A. L., Lonneman, W. A., Docherty, K. S., Jaoui, M., Pye, H. O. T., Hu, W., Day, D. A., Campuzano-Jost, P., Jimenez, J. L., Guo, H., Weber, R. J., de Gouw, J., Koss, A. R., Edgerton, E. S., Brune, W., Mohr, C., Lopez-Hilfiker, F. D., Lutz, A., Kreisberg, N. M., Spielman, S. R., Hering, S. V., Wilson, K. R., Thornton, J. A., and Goldstein, A. H.: Monoterpenes are the

largest source of summertime organic aerosol in the southeastern United States, P. Natl. Acad. Sci. USA, 115, 2038–2043, https://doi.org/10.1073/pnas.1717513115, 2018.

Zhao, D., Schmitt, S. H., Wang, M., Acir, I.-H., Tillmann, R., Tan, Z., Novelli, A., Fuchs, H., Pullinen, I., Wegener, R., Rohrer, F., Wildt, J., Kiendler-Scharr, A., Wahner, A., and Mentel, T. F.: Effects of NO_x and SO_2 on the secondary organic aerosol formation from photooxidation of α-pinene and limonene, Atmos. Chem. Phys., 18, 1611–1628, https://doi.org/10.5194/acp-18-1611-2018, 2018.

Zhao, D., Pullinen, I., Fuchs, H., Schrade, S., Wu, R., Acir, I.-H., Tillmann, R., Rohrer, F., Wildt, J., Guo, Y., Kiendler-Scharr, A., Wahner, A., Kang, S., Vereecken, L., and Mentel, T. F.: Highly oxygenated organic molecule (HOM) formation in the isoprene oxidation by NO_3 radical, Atmos. Chem. Phys., 21, 9681–9704, https://doi.org/10.5194/acp-21-9681-2021, 2021.

Zhao, D. F., Buchholz, A., Kortner, B., Schlag, P., Rubach, F., Kiendler-Scharr, A., Tillmann, R., Wahner, A., Flores, J. M., Rudich, Y., Watne, Å. K., Hallquist, M., Wildt, J., and Mentel, T. F.: Size-dependent hygroscopicity parameter (κ) and chemical composition of secondary organic cloud condensation nuclei, Geophys. Res. Lett., 42, 10920–10928, https://doi.org/10.1002/2015gl066497, 2015a.

Zhao, D. F., Kaminski, M., Schlag, P., Fuchs, H., Acir, I.-H., Bohn, B., Häseler, R., Kiendler-Scharr, A., Rohrer, F., Tillmann, R., Wang, M. J., Wegener, R., Wildt, J., Wahner, A., and Mentel, Th. F.: Secondary organic aerosol formation from hydroxyl radical oxidation and ozonolysis of monoterpenes, Atmos. Chem. Phys., 15, 991–1012, https://doi.org/10.5194/acp-15-991-2015, 2015b.

Zhou, L., Gierens, R., Sogachev, A., Mogensen, D., Ortega, J., Smith, J. N., Harley, P. C., Prenni, A. J., Levin, E. J. T., Turnipseed, A., Rusanen, A., Smolander, S., Guenther, A. B., Kulmala, M., Karl, T., and Boy, M.: Contribution from biogenic organic compounds to particle growth during the 2010 BEACHON-ROCS campaign in a Colorado temperate needleleaf forest, Atmos. Chem. Phys., 15, 8643–8656, https://doi.org/10.5194/acp-15-8643-2015, 2015.

Ziemann, P. J. and Atkinson, R.: Kinetics, products, and mechanisms of secondary organic aerosol formation, Chem. Soc. Rev., 41, 6582–6605, https://doi.org/10.1039/c2cs35122f, 2012.